Electronic Properties of $NiS_{2-x}Se_x$ Single Crystals: From Magnetic Mott−Hubbard Insulators to Normal Metals

J. M. Honig*

Department of Chemistry, Purdue University, West Lafayette, IN 47907-1393

Jozef Spałek

Marian Smoluchowski Institute of Physics, Jagiellonian University, ulica Reymonta 4, 30-059 Kraków, Poland

Received May 19, 1998. Revised Manuscript Received September 8, 1998

The $NiS_{2-x}Se_x$ system represents one of the best examples of a Mott−Hubbard system, i.e. a system in which, under appropriate conditions of concentration, temperature, or pressure, a metal−insulator transition driven by electron−electron interaction takes place. Here, the metallic phase is either antiferromagnetic (for $0.44 \leq x \leq 1$) or paramagnetic (for $x \geq 1$), whereas the insulating phase is as a rule antiferromagnetic (including the spin-canted phases). In this paper we review both the physical properties and outline the basic features of the theoretical approach to those *correlated electron systems*. Emphasis is placed on a qualitative understanding of the observed transformation of the system from semiconductor (or magnetic insulator) to metal.

Contents

I. Introductory Remarks

We review below the synthesis, characterization, physical properties, and theoretical analysis of the $NiS_{2-x}Se_x$ system; by now substantial literature has accumulated on the subject. Space limitations preclude a complete review of all the relevant publications. The work carried out on NiS_2 up to 1985 has been thoroughly reviewed by Wilson;[1] relatively little additional work has been done on this end member of the series since then. We therefore primarily concentrate on the $NiS_{2-x}Se_x$ systems with variable S/Se ratios and on the *physical* interpretation of the results. At the end we list several new and unresolved problems in the field.

As is emphasized below, the $NiS_{2-x}Se_x$ system is a paradigm for materials whose physical properties can be substantially altered by relatively small compositional changes: in particular, as is shown on the phase diagram displayed in Figure 1, the alloy changes from a magnetic insulator to a metal with increasing Se content; also, magnetic ordering of several types can be induced by lowering the temperature. What sets this particular system apart from almost any others with similar characteristics is that remarkable changes in electrical and related properties can be achieved by alterations in the anion sublattice, while the cation sublattice is kept intact. This comes about because NiS_2 is a good insulator, whereas $NiSe_2$ is metallic; these two components can be mixed in all proportions, whereby a continuous changeover from one regime to the other is achieved. Thus, one anticipates interesting electrical and magnetic anomalies close to the critical range of x values where a phase transition from the insulating to the metallic phase occurs. By contrast, in most other systems such alterations are induced by cationic substitution of altervalent substituents (e.g., $(V_{1-x}Cr_x)_2O_3$) or through changes in anion/cation ratios (e.g. $V_{2(1-\delta)}O_3$), both of which disturb the lattice periodicity. In all these

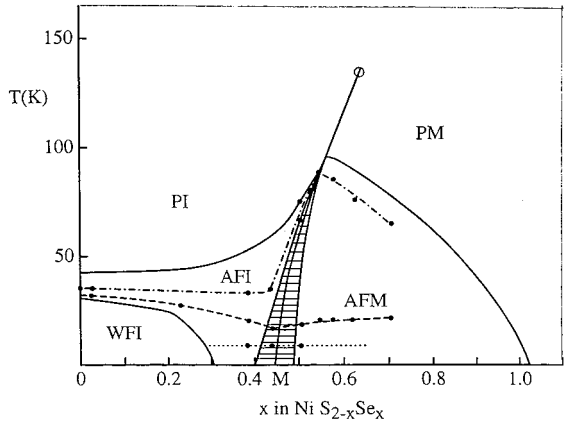

Figure 1. Phase diagram for the $NiS_{2-x}Se_x$ system. The placement of the phase boundaries is uncertain. Solid curves represent boundaries inferred from a fairing of the available literature data. Dashed and dotted curves and points represent recent data from refs 7 and 32. PI, paramagnetic insulator; PM, paramagnetic metal; AFI, antiferromagnetic insulator; AFM, antiferromagnetic metal; WFI, weak ferromagnetic insulator (actually, canted antiferromagnetic insulator).

10.1021/cm9803509 CCC: $15.00
Published on Web 10/19/1998

cases a transition from the insulator to the metal occurs at a sharply defined concentration x.

As has been emphasized by theorists in the field, it is fundamentally important to search for and study single valence systems that display transitions from a weakly to a strongly correlated electron regime. This has motivated a renewed interest in the nickel disulfide−diselenide system. There is an added incentive to renewed studies: in these $NiS_{2-x}Se_x$ alloys neither changes in Se content nor variations in magnetic order perceptibly alter the crystal structure. This permits us to study changes in electronic properties through compositional alterations without interference from variations in lattice properties.

In short, the chemical and physical characteristics of this system are not only of intrinsic interest but they also provide experimental inputs for a theoretical problem of great contemporary significance: how to handle the description of strongly interacting electrons when the standard band theory is no longer applicable. The $NiS_{2-x}Se_x$ system is a testing ground for such descriptions. Accordingly, we will emphasize the interplay between experimental measurements and theoretical analysis. However, in presenting the theory we will minimize the mathematical derivations, which are described in the original publications in great detail, and concentrate instead on the final results that are useful in the analysis of experimental data.

Historically, aside from one pioneering study,[2] most of the seminal work on the alloys was carried out by the DuPont group[3−6] who, in the period from 1968 to 1973 published experimental work dealing with the synthesis, single crystal growth, and characterization of the alloys, principally over the range $0 \leq x \leq 0.6$. Their resistivity curves called attention to the complexities of the $NiS_{2-x}Se_x$ system, which resulted in much follow-up work in the ensuing decades. The DuPont group also proposed a phase diagram on the basis of their resistivity, X-ray, magnetization, and heat capacity measurements. This was later somewhat modified by other investigators as described below. A version which interpolates between the various different reports is presented in Figure 1. There is general agreement as to the location of the different phases on the temperature vs composition diagram. However, the precise positioning of the phase boundaries is still uncertain, owing to discrepancies among the various investigators. The latest data, as reported in ref 7, are indicated by the experimental points and dotted or dashed lines in Figure 1. As anticipated, when x is increased, the system becomes increasingly metallic; also, with rising temperature one proceeds from magnetically ordered to disordered phases. One should carefully note the different phases that are encountered as x and T are altered; these involve canted-spin (or weak-ferromagnetic) (WFI), antiferromagnetic (AFI), and paramagnetic (PI) insulators and antiferromagnetic (AFM) and paramagnetic (PM) metals.

The principal features of this phase diagram are the following: (1) There is a phase transition, usually of first-order, between the metallic and insulating regimes. (2) For a particular set of compositions, the transition from the metallic to the insulating phase occurs with increasing temperature; this is a rather unusual circumstance with which we deal later. (3) At relatively low temperatures the alloys are antiferromagnetically ordered, both on the insulating and on the metallic side; at cryogenic temperatures and over a limited range of x the solid solutions display weak ferromagnetism. In addition, (4) the magnetic moments of the insulating compounds are significant, whereas those of the metallic phase are much smaller. (5) The resistivity of the metallic phase close to the localization limit and at low temperature varies as T^2. Concomitantly, the electronic contribution to the heat capacity and the magnetic susceptibility are both much larger than in conventional metals. These particular features represent signatures of a system of correlated electrons.

The Mott−Hubbard transition plays a fundamental role in the physical transformation of atomic states into itinerant (band) states. The theory outlined in section V represents an attempt to rationalize the data described in sections IV.A−E within the framework of current models of electron correlation effects. This is based on the central concept that the metal−insulator boundary represents a delocalization−localization line pertaining to the 3d electronic states of these compounds. In other words, the 3d states on the insulating side are atomic-like, obeying Hund's rule, whereas those on the metallic side represent Bloch-type states or, more precisely, constitute a Fermi liquid. In such a situation an immediate question arises: how can a thermal stimulus of 50−100 K give rise to such a drastic alteration in the nature of the electronic states which involve an energy scale of 1−2 eV? We shall see that this can result from a balancing out of the Coulomb repulsion between interacting electrons that almost compensates the band energy of the 3d electrons in narrow band states.

II. Band Structure Schemes

A. General Scheme. The interpretation of experimental data depends on the availability of a band structure scheme for the $NiS_{2-x}Se_x$ system. Present quantitative evaluations are still at a somewhat rudimentary stage, because of the difficulty of taking electron correlation effects into account, but an outline is beginning to emerge, and with time the accuracy of current calculational efforts is bound to improve.

Goodenough[8,9] provided a conceptual framework for ordering the bands for electrons of topmost energy in materials with pyrite structures. He classified electrons as being involved in the formation of anionic molecular states $(SS)^{-2}$, in bands of primarily t_{2g} character that do not hybridize strongly with the anionic states, and in bands formed by strong σ-type bonding between cations and anions. Brief mention was made[10] of the band structure of NiS_2, in an extension of the tight binding methodology as applied to FeS_2. Later work by Bullett[11] provided a quantitative rationale obtained in the local density approximation, with neglect of charge transfer between cations and anions. The resulting schematic diagram of band edge limits is shown for various pyrite structures in Figure 2. As is seen, nickel disulfide is predicted to be metallic, in serious disagreement with experimental results, but the scheme is nevertheless useful for indicating the distinctions between NiS_2 and the other disulfides with pyrite struc-

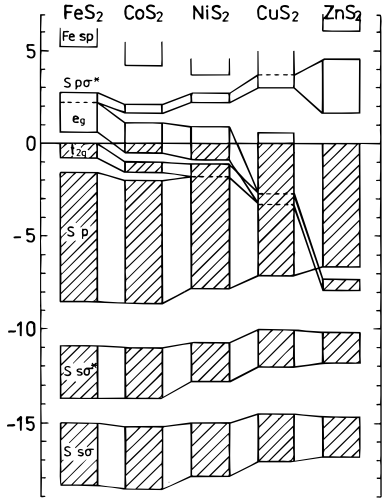

Figure 2. Schematic band structure diagram for the indicated disulfides. Note the half-filling of the e_g band in NiS_2. Adapted from ref 11.

ture. Furthermore, the fact that the e_g band in NiS_2 is half-filled suggests that there is built in an instability which can lead to the opening of a Mott−Hubbard band gap when electron correlations are taken into account. This work was extended[12] using a self-consistent charge, a linear combination of atomic orbitals, and the X_α procedure. These calculation again show the Fermi level intersecting the Ni e_g band approximately at the midpoint. This clearly shows the need to go beyond the local density approximation, to incorporate electron correlation effects. As far as can be ascertained, no density functional calculations have been published do date.

In an alternative approach, configuration interaction calculations have been performed for the energy levels of small clusters by simulating the crystal and then adjusting the parameters for an optimal fit of the cluster energies to available XPS core level photoemission spectra.[13] NiS_2 was only one of a number of compounds treated in this manner to discern the trends existing for many transition metal compounds. Subject to several limitations discussed in the article, values were cited for the charge transfer energy $\Delta = 2$ eV, for the Hubbard repulsion energy $U = 2$ eV, and for the cation−anion overlap integral $t = -1.1$ eV. One must clearly keep in mind that Δ and U were defined with respect to the center of gravity of their respective multiplets, so that the gap energies, reduced by the appropriate band widths, are considerably smaller. The above approach was subsequently refined[14] by introduction of two additional parameters related to the thermal promotion of charge carriers from the ligands and from the central Ni atom to the conduction band; however, it is difficult to decide from among several alternative parametrizations that were presented which one produces the optimal fit to experimental XPS data.

In these circumstances we confine ourselves to a brief discussion of the qualitative aspects of the band structure. Several options are presented in Figure 3. In part a we show the overall disposition of bands close to the Fermi level: the ppσ and ppσ* narrow bands represent the bonding and antibonding configurations of the $(SS)^{-2}$ unit, augmented by bonding to the e_g state of Ni. The pσ and pσ* parts are the 3p energy bands for sulfur. The narrow t_{2g} bands represent Ni states that bond only weakly to anionic neighbors. Lastly, we show schematically the half-filled band of e_g states in the absence of electron correlations. As is well-established, correlation effects are expected to split this band into subbands. One may then encounter the Mott−Hubbard configuration depicted in part b, where both halves lie above the 3pσ sulfur band; the intraatomic repulsion energy U is smaller than the energy difference Δ between the top of the 3pσ* and the bottom of the e_g* bands. This is a manifestation of the well-known Mott−Hubbard insulator arising from electron correlations. One thereby immediately rationalizes the fact that NiS_2 is a good insulator at low temperatures. An alternative disposition is shown in part c, where $\Delta < U$, so that thermal excitations of electrons occur across the gap between the 3pσ* and e_g states. This is a manifestation of a charge transfer insulator of the type described by Zaanen et al.[15] Opinion is divided as to which category is appropriate for NiS_2. Bocquet and co-workers[14] strongly argue in favor of the latter alternative, but their evidence is indirect and not in accord with thermoelectric effects described below. Lastly, in part d we depict the case where Δ slightly exceeds U, such that at low temperatures the compound is a Mott−Hubbard insulator and at higher temperature the charge transfer effects become manifest. We believe that this representation is appropriate to the $NiS_{2-x}Se_x$ system, as described below.

B. Experimental Investigation of Band Structures. Experimental information concerning the band structures of the $NiS_{2-x}Se_x$ system derives principally from photoelectron spectroscopy. Early work[16] involved X ray photoelectron spectroscopic (XPS) studies in the range 0−25 eV below the Fermi level E_f for NiS_2 at 300 K. The S 3p and Ni 3d bands were found to overlap in this range of energies. UV photoemission experiments via synchrotron radiation on NiS_2 showed[17] a shoulder near the Fermi energy E_f, assigned to e_g states which were separated by roughly 2 eV from lower lying t_{2g} states and merged with the S 3p band. In XPS measurements on the $NiS_{2-x}Se_x$ system with $x = 0$, 0.2, 0.475, 0.9, and 2, Krill and Amamou[18] detected a noticeable shift of the anionic p band towards E_f with increasing x, thus validating the hypothesis introduced by us earlier. Their UPS studies in the range 0−2eV did not indicate any drastic change in the 1 eV energy separation between the t_{2g} and e_g bands or any shift with respect to E_f when the Se content was changed. Both XPS and BIS (bremsstrahlung isochromat spectroscopy) measurements[19] near E_f provided a resolution of the band structure above as well as below E_f, with moderate resolution for alloys with $x = 0$, 0.8. Spectra of the core level for the Ni $p_{3/2}$ state were also studied; a complementary study of the S 2p spectrum is also available.[20] A detailed investigation via angle resolved photoemission spectroscopy[21] of the compounds with $x = 0$ and 0.5, shown in Figures 4 and 5, is of special interest: it shows the presence of a band very close to E_f in the alloy which is absent from pure NiS_2. Moreover, the leading edge of this band closely tracked the resistivity of the alloy over the temperature range 25−120 K. As indicated below, a metal insulator transition occurs in this material with rising T over the interval

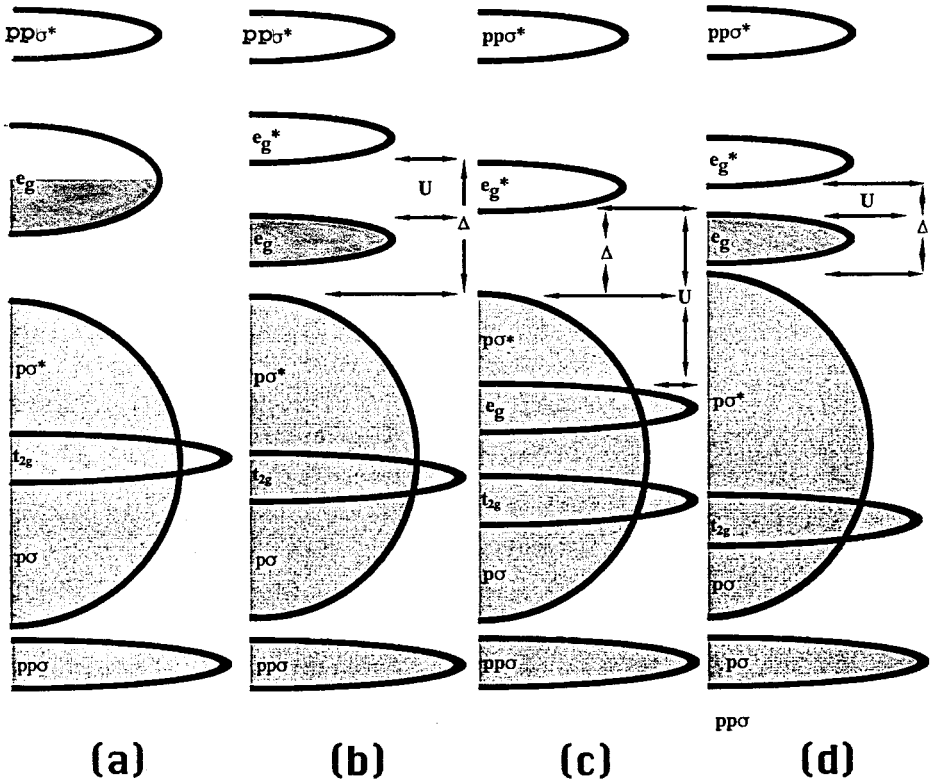

Figure 3. Proposed qualitative band structure diagram for the $NiS_{2-x}Se_x$ system. See text for details. Shaded areas represent occupied states.

55−65 K; this is accompanied in the same range by a shift of the e_g levels towards E_f, a direct indication of a bona fide transition due to the disappearance of a band gap. Furthermore, the systematic shift with increasing temperature of the band away from the Fermi energy means that there is no residual density of states in the middle of the Hubbard gap as the system is driven toward the insulating state. This behavior is in disagreement with recent theoretical predictions concerning the existence of such residual states. Lastly, a UPS investigation[22] of NiS_2 spectra in the 0−16 and 50−80 eV range has established that the shoulder at 5 eV is due to a d^7 final state involved in the excitation, whereas the main band represents a final $d^8\underline{L}$ state. The authors stress their belief that the highest occupied state is S 3p-like, and not Ni 3d-like. This need not be in conflict with the thermoelectric data requirements. One must remember that the intensity of d−d* transitions under UPS excitations is much weaker than the intensity of p−d* transitions. Hence, if the S 3p and Ni 3d band edges are energetically proximate, the intense transitions will tend to mask the weaker ones. Then, so long as the S 3p states lie slightly below the Ni 3d states, the electrical measurements at low temperatures are governed by the d−d* energy separation, while the UPS measurements involve 3p−3d energy differences.

Very careful, systematic studies of the energy band structures and their changes with Se substitution in NiS_2 are still urgently needed.

III. Sample Preparation of $NiS_{2-x}Se_x$

As always, the adequate preparation of samples in single crystal form is a prerequisite for a proper study of the system of interest. The preferred methodology for the preparation of $NiS_{2-x}Se_x$ is the ceramic technique of reacting Ni, S, and Se in appropriate amounts at elevated temperatures, followed by repeated grindings and firings. Alternatively, chemistry variants, using precursor synthetic routes, have been employed.[23−26] The reaction of Na_2S_5 with K_2NiF_6 at 65 °C resulted in products of good crystallinity.[24] Alternatively, $NiO(OH)_2$ or its hydrate may be used in conjunction with Na_2S_5 in liquid NH_3, or with ammonium polysulfide or thioacetamides in appropriate solvents to obtain crystalline products after gentle heating.[25] Combination of the elements in liquid NH_3 in a pressurized vessel, followed by gentle warming, has also proven successful.[26]

Single crystals have generally been grown by chemical vapor transport techniques.[3,4,6,27] A difficulty in this procedure is the incorporation into the lattice of the transporting agent in non-negligible amounts, which leads to unintentional doping effects. This problem may be prevented by growth of NiS_2 crystals from alkali polysulfide fluxes[28] or by exposing previously prepared NiS to sulfur vapor in a two-zone furnace. The sublimation process requires on the order of several days.[29] Deviations from ideal stoichiometry in this latter process can be regulated by adjustment of the sulfur vapor pressure. However, it is not clear whether the procedure could be extended to produce intermediate S/Se compositions.

Unintentional doping may also be circumvented by use of Te as a flux; under controlled conditions, crystals 4−5 mm on an edge can be obtained.[30] On account of

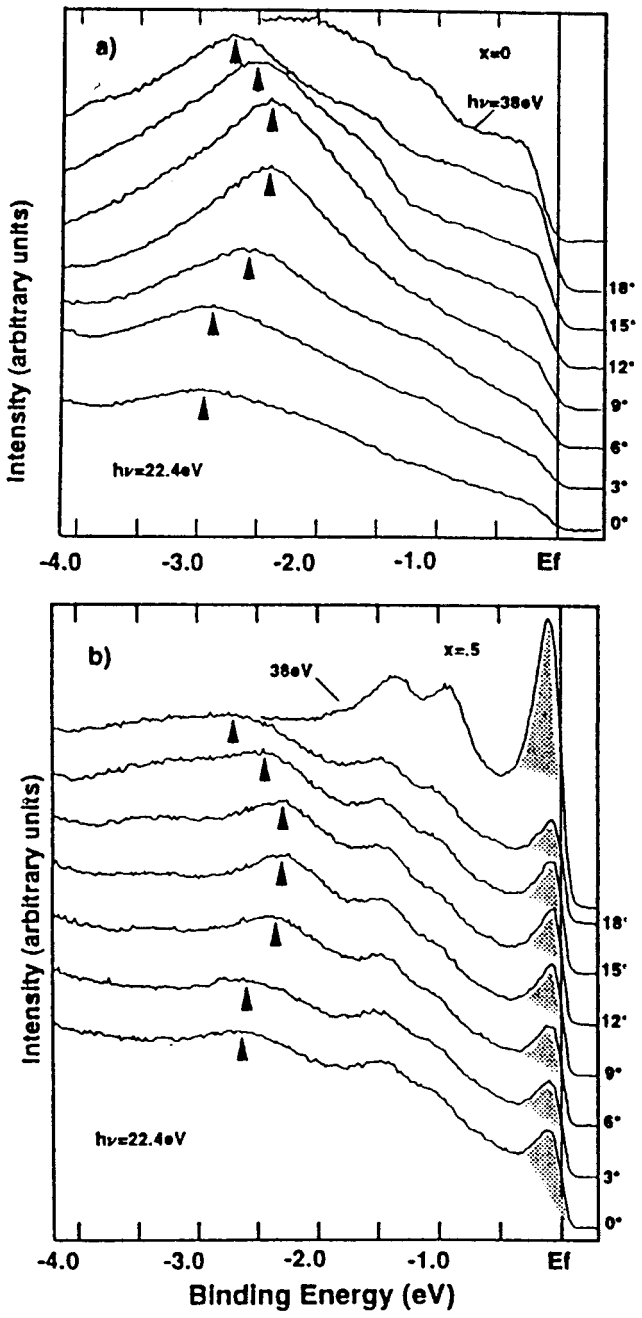

Figure 4. Valence band UPS spectra of NiS_2 (a) and of $NiS_{1.5}Se_{0.5}$ (b). Note the extra peak in the latter spectrum. After ref 21.

its large size, Te does not enter the lattice in detectable amounts. Details are provided elsewhere.[30,31] Indeed, samples with compositions $0 \leq x \leq 0.4$ as prepared by the flux method exhibit much higher resistivities[32] than do those prepared by the vapor transport method.

What is still not subject to adequate experimental control is the anion/cation ratio $r = [S+Se]/[Ni]$. Even small deviations from the ideal ratio $r = 2.000$ are equivalent to extensive changes in the charge carrier density. The problem here is to find any technique by which r may be determined to at least four significant figures; electron microprobe or conventional wet chemical techniques are not equal to this task. The problem is manifest not so much in the variations of the lattice parameter of NiS_2 as in most other physical quantities, such as electric and magnetic properties for NiS_2 under pressure[33] or ambient conditions[34] and the Moessbauer effect.[35] Research in this area was carried out on NiS_d samples with $1.93 < d < 2.09$, whose composition was analyzed by the wet chemical techniques detailed in ref 35. The S/Se ratio may also be conveniently determined by electron microprobe techniques, calibrated against NiS_2 and $NiSe_2$, as has been done in recent work.[32] By rastering the beam across the sample it can be established whether this ratio remains constant and close to the ideal value of 2 within experimental error for any given crystal. Unfortunately, this method also suffers from fairly significant experimental uncertainties; the quantity d is known only to within ± 0.005 units.

The major stoichiometry effects are seen in electrical and magnetic properties, as reported in several studies on NiS_2 by Krill and co-workers:[33−35] the resistivities decrease by as much as 2 orders of magnitude and the magnetic susceptibilities, by a factor of 3, as r is raised from 1.91 to 2.14. These results clearly demonstrate the need for proper control over sample composition to establish the physical characteristics of stoichiometric NiS_2. As another instance, one may cite the transition from the magnetically ordered metallic to the magnetically ordered insulating state of one polycrystalline sample of composition $x = 0.52$. Sudo[36] reported that the transformation for one of his ceramic samples was first order, as judged by the discontinuity in resistivity and by the near discontinuity in magnetic susceptibility, as well as by appreciable hysteresis effects. By contrast, most other investigators, including the present authors, report more gradual resistivity changes for single crystals in that composition range. One may ascribe this difference to the better sample preparation method employed by Sudo. Nevertheless, the results cited below for less perfect specimens are still of intrinsic interest. They demonstrate that such samples provide an excellent testing ground for the experimental study of electron correlation phenomena. However, the adequate control of sample composition is an outstanding problem that must still be adequately resolved.

Raman spectroscopy has been used[37,38] to document the presence of bond stretching vibrations assigned to S−S, S−Se, and Se−Se molecular units. This indicates that there is a quasi-random distribution of Se for S in the anionic pairs of the pyrite structure shown in Figure 6, along with the nearest neighbor configurations for both cations and anions. The interionic axes of the diatomic chalcogenides are oriented along the various {111} directions of the cubic unit cell.

IV. Physical Properties

A. Electrical Properties. The electrical characteristics of the $NiS_{2-x}Se_x$ system were first systematically explored by the DuPont group,[5] who investigated the resistivity (ρ) of single crystals grown by the vapor transport technique. Subsequent investigations,[32,36,39−45] both on single crystals and on polycrystalline materials, are in reasonable agreement with the pioneering study and with each other. We show in Figures 7 and 8 recent studies on single crystals in the range $0 \leq x \leq 0.71$[32] and on polycrystalline alloys in the range $0.7 \leq x \leq 1.2$[39] as representative of the entire group. Four regimes may be distinguished.

(i) $0 \leq x \leq 0.38$: Samples in this composition range are insulators (semiconductors). Their resistivities drop

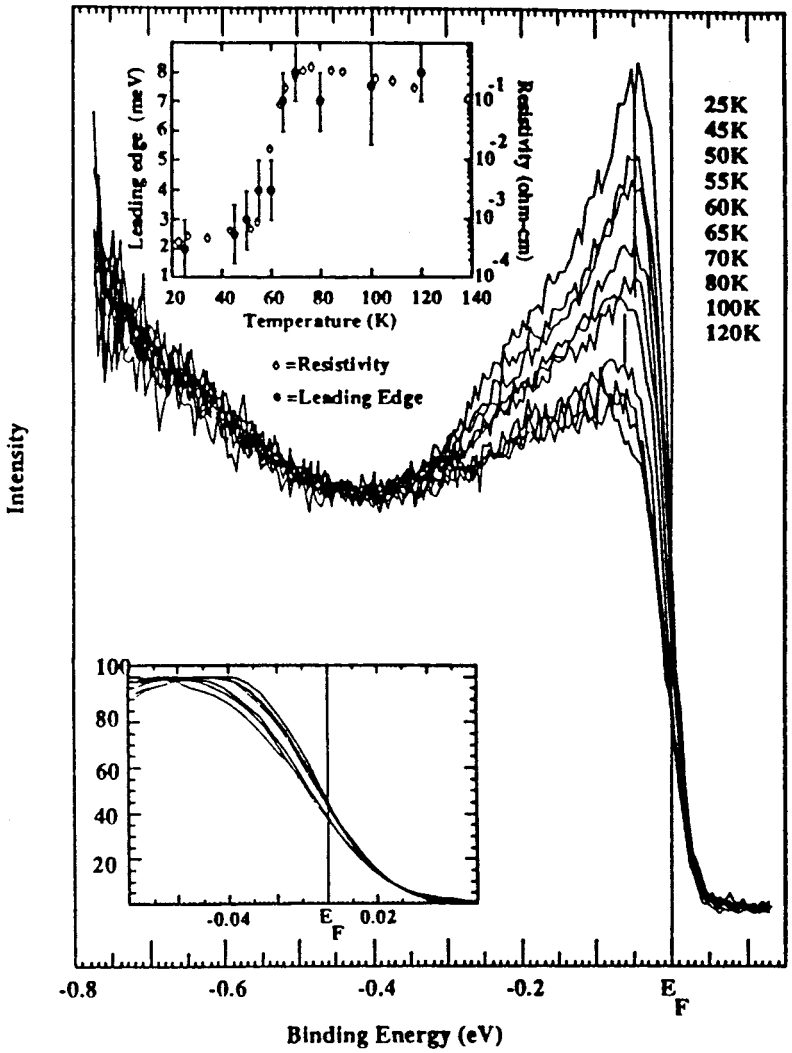

Figure 5. Temperature dependence of the UPS absorption peak near the Fermi level. Note the parallel between the leading edge position and the resistivity as a function of temperature, as shown in the upper inset. In the lower inset is documented the clustering of spectra for metallic and nonmetallic alloys. The ordering of the curves matches the temperature listings. After ref 21.

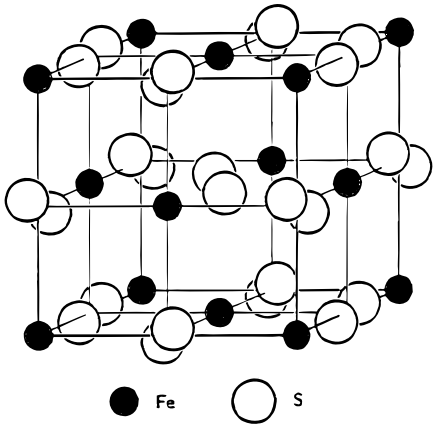

Figure 6. Crystal structure of pyrite, isomorphic with $NiS_{2-x}Se_x$.

exponentially with rising temperature in the range below 30 K, where the alloys are weakly ferromagnetic. From the linear plots of log ρ vs $1/T$ one estimates an activation energy of 330 meV. Between 50 and 150 K ρ remains at a plateau. Beyond this temperature, the resistivity again drops exponentially with rising temperature, characterized by an activation energy of 110 meV. Both gap sizes are independent of composition.

(ii) $0.38 \leq x \leq 0.51$: Alloys of this composition are "metallic" at low temperatures in the sense that ρ is "small" and nearly independent of T. The resistivities extrapolated to 0 K, ρ_0, vary from roughly 1 Ω cm (an astonishingly high value, six orders of magnitude above that of impure copper) at the lower composition limit, to 10^{-3} Ω cm at the upper limit (still a rather high value for a metal). This is followed by a very steep rise in resistivity in the range 50−70 K, culminating in a maximum, which for some compositions exceeds ρ_0 by a factor of 700. Beyond this maximum, ρ again drops exponentially with rising T, with a corresponding activation energy of 110 meV, the same as for regime i.

(iii) $0.55 \leq x \leq 0.64$: One encounters a metallic state below 50 K, which is followed by a shallow maximum spread out over a wide temperature range, beyond which the resistivity once more drops slowly with rising temperature.

(iv) $0.65 \leq x \leq 2$: The system remains metallic,[41] that is, the resistivity rises with temperature but remains in the range below 10^{-3} Ω cm.

All alloys in the metallic region for regimes ii−iv display the same temperature variation: At low T, $\rho =$

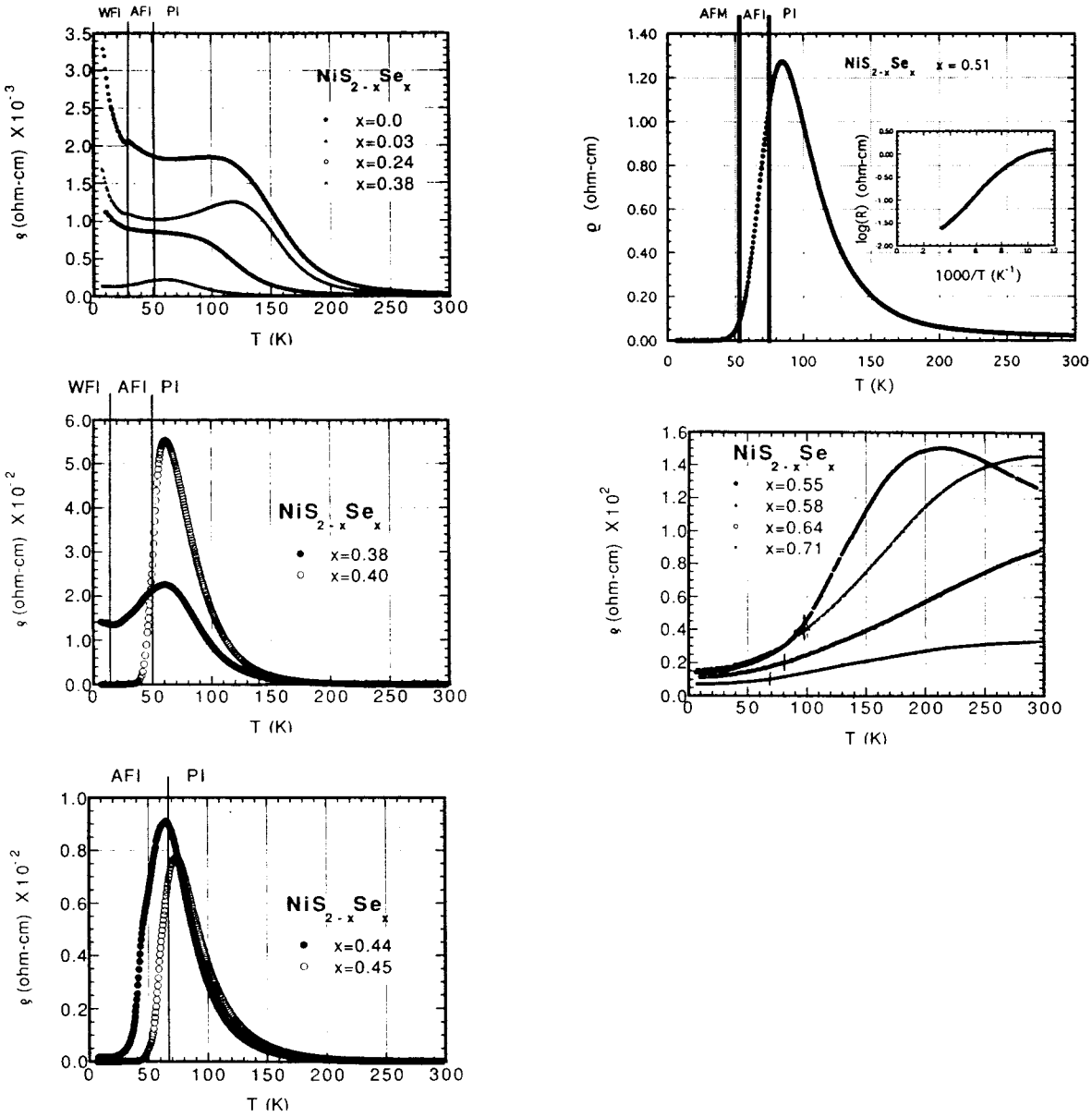

Figure 7. Electrical resistivities of $NiS_{2-x}Se_x$ single crystals in various composition ranges, $x < 0.75$. The ordering of the curves matches the listing of x values. After ref 32.

$\rho_0 + AT^2$; A remains in the range 2−4 nΩ cm/K^2, except near $x = 1$, where A peaks near 14 nΩ cm/K^2.[43,45] This type of T dependence is one of the signatures of electron correlation effects that will be discussed in section V. At moderate temperatures the variation of ρ with T is linear, comparable to that encountered in the normal range of many high T_C superconductors. The above features will be rationalized in later sections.

Hall coefficients (R) have been probed in several studies: Thio and Bennet[46] investigated different sample geometries and concluded that that surface layers in single crystals of NiS_2 complicate the interpretation of the phenomenon. A systematic study has recently been reported by Takagi and co-workers[43,45] for single crystals of compositions between $x = 0.5$ and 2. This coefficient assumes the essentially constant value of $R = +10^{-4}$ cm^3/C above 200 K for all specimens. This is consistent with a density of two charge carriers/Ni. The authors do not attempt to draw a distinction between the ordinary and extraordinary components of R in the magnetically ordered range of temperature, but they do regard the large rise of R with diminishing T below 200 K as an indication of a shrinking Fermi surface as a concomitant to the Slater splitting of the conduction band when magnetic ordering prevails. Unfortunately, due to the complexities of the band structure, no unambiguous determination of the charge carrier mobilities could be attempted.

Thermoelectric measurements are quite instructive; two systematic studies[32,41] yielded largely concordant results. Figure 9 demonstrates an apparent anomaly, in that the Seebeck coefficient α for alloys in regime i is very small at low temperatures. This violates the general rule of thumb that α should rise with increasing resistivity. This apparent anomaly may be explained by postulating that the Fermi surface of the alloys is complicated and contains both hole and electron pockets in reciprocal space. From quite general thermodynamic principles one can show[47] that for materials in which both electrons and holes participate in transport pro-

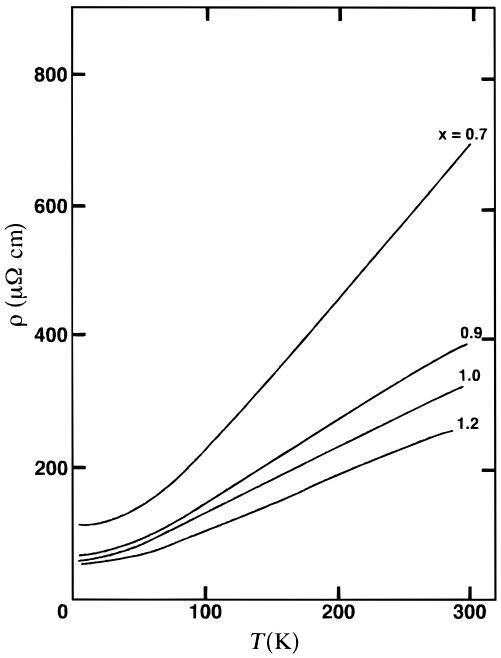

Figure 8. Electrical resistivities of polycrystalline $NiS_{2-x}Se_x$ in the indicated composition range. Adapted from ref 39.

cesses the Seebeck coefficient is specified by

$$\alpha = \frac{-|\alpha_n|\sigma_n + \alpha_p\sigma_p}{\sigma_n + \sigma_p} \qquad (4.1)$$

where α_n and α_p are the partial Seebeck coefficients and σ_n and σ_p are the partial conductivities of electrons and holes respectively. One sees that when the material is nearly intrinsic the positive and negative contributions in the numerator nearly cancel out, rendering α small, even though the separate contributions α_n and α_p may be numerically large. One may check on this hypothesis by plotting α/ρ vs T; according to eq 4.1 this ratio should be close to zero for nearly intrinsic materials. Plots of this type[32] show that this is indeed the case for all compounds classified in category i and ii for temperatures below 120−150 K. One may anticipate such properties for Mott−Hubbard insulators where the conduction band is split by correlation effects into nearly mirror image subbands, as discussed earlier with reference to Figure 3b. However, this scenario is not in accord with recent analyses which suggest that the $NiS_{2-x}Se_x$ system should be classified as a charge transfer system,[13,21,22] as depicted in Figure 3c. However, as discussed earlier, it is not implausible to assume the scenario depicted in Figure 3d, where the upper band edges of the $3de_g$ lower subband of Ni and of the 3p valence band of sulfur are shown as being very close in energy, so that Δ exceeds U only marginally. Then at low temperatures the thermal excitations involve the Hubbard subbands, as before, but as the temperature rises the S $3p\sigma^*$−Ni e_g^* excitations become increasingly prominent. In fact, as is evident from Figure 9, deviations of α from their very low values become noticeable above 150 K, i.e., in the range where the alloys begin to show comparatively low resistivities. When k_BT becomes comparable to Δ, the contributions $-|\alpha_n|\sigma_n$ and $\alpha_p\sigma_p$ still roughly cancel out, but now the additional contributions to α from the carriers in the relatively

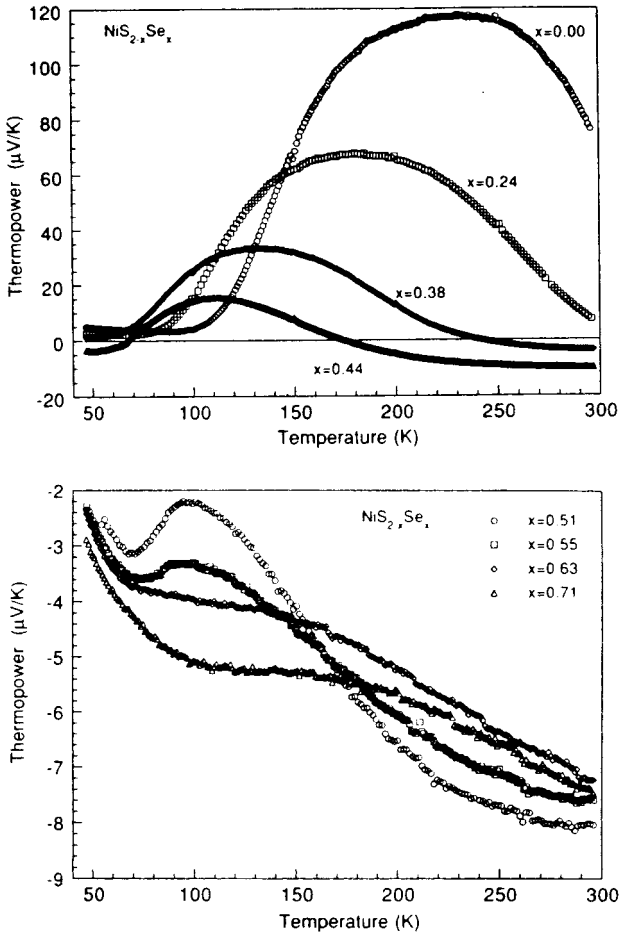

Figure 9. Seebeck coefficient measurements on $NiS_{2-x}Se_x$ single crystals for $x < 0.5$. The ordering of the curves at 100 K matches the listing of the x values. After ref 32.

wider S $3p\sigma$ band begin to be increasingly effective. The α values now fall in the range anticipated for semiconductors in which hole transport in a single band dominates. The rising trend of α with T is ultimately interrupted by the continuing increase in density of high mobility charge carriers with rising T. This renders the alloys more metallic and thereby decreases α, thus forcing the Seebeck coefficient to go through a maximum.

A somewhat similar explanation is expected to hold for materials in category ii: With increasing admixtures of Se the σ-type interactions between the Ni e_g and anionic p states is expected to increase, thereby lowering the p band with respect to the e_g band. This increases Δ in Figure 3d. Thus, at low temperatures the electronic features are determined primarily by the Hubbard gap: α remains small in the range of temperatures where the alloys are quasimetallic. When the electron correlations force an opening of the e_g band into nearly symmetric Hubbard subbands, the alloys remain essentially intrinsic; eq 4.1 is expected to hold, so that the sharp rise of ρ with T in Figure 7b,c is not mirrored in the Seebeck data. Continued excitation of charge carriers across the Hubbard gap U does not fundamentally alter this situation; α remains small throughout the temperature range under study.

Finally, compounds in regimes iii and iv are sufficiently metallic that α remains small throughout. The standard theoretical analysis[47] shows that α is expected

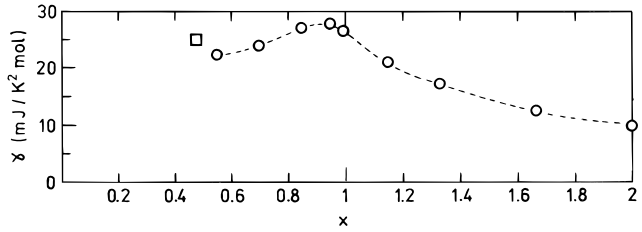

Figure 10. Values of the electronic contribution to the heat capacity of $NiS_{2-x}Se_x$ for $x = 0.5$. After ref 45. The square symbol refers to unpublished measurements of Kim et al.

to vary as $1/T$, which is indeed found to be the case; the scale of ordinates showing this effect in Figure 9 exaggerates the fluctuations at the microvolt scale.

B. Heat Capacity Studies. Several heat capacity (C) investigations have been reported for NiS_2 and $NiSe_2$,[48,49] for alloys with $x = 0.51$, 0.52,[52,53] as well as for several intermediate compositions.[45,50,51]

Heat capacity anomalies have been reported at the various phase transitions. However, values for the concomitant transition entropies differ considerably because of the difficulty of properly subtracting the baseline to determine the excess heat capacity. The Japanese groups have referred their measurements to the best calculated Debye curve that fit their data below 10 and above 70 K; Yao and co-workers opted to draw a baseline more conservatively to bracket only the temperature range in the immediate vicinity of the anomaly. Thus, depending on the sample composition and baseline subtraction method, the reported values for the entropy of transition from the ferro- to the antiferromagnetic state or from the magnetically ordered to the disordered state range between 0.75−2.5 and 5.8 J/molK, the latter value being close to R ln 2. The upper limit seems to be unrealistic; for, the observed heat capacity fell above the calculated Debye curve between 10 and 80 K, whereas a sharp peak was registered only over a 15 K temperature interval. If one eliminates the highest cited values, the entropy of transition is generally far less than that anticipated through the relation R ln $(2S + 1)$.

Of great interest is the electronic contribution (γ) to the heat capacity for the metallic phase in the composition range $0.5 \leq x \leq 2$, as determined from low-temperature heat capacity measurements. As is well-established, elementary theories show that $C = \gamma T + aT^3$, where the aT^3 is the contribution anticipated for lattice and antiferromagnetic magnon excitations. Accordingly, plots of C/T vs T^2 should be linear, with the intercept yielding the value of γ. Actually, such plots are never quite linear for the $NiS_{2-x}Se_x$ system. Observed curvatures have been tentatively attributed to spin fluctuations.[52,53] Departures from the C/T vs T^2 linearity at low temperatures (<6 K)[51] have also been related to an unspecified transition; this possibility must be further investigated. Despite such problems, the γ values obtained by extrapolation from the essentially linear regions to the intercept, as carried out by the various investigators, are in reasonable agreement. We show in Figure 10 a recent compilation of γ values for $x > 0.5$[45] (note one additional point for $x = 0.44$); it is seen that the electronic contributions for the alloys are higher by a factor of up to 3 compared to the value $\gamma =$ 9 mJ/mol K^2 for $NiSe_2$, which is a poor metal. As shown in section V, this enhancement can again be directly linked to electron correlation phenomena, repeatedly invoked for alloys of intermediate composition x. It is of interest that γ peaks near $x = 1$ and 0.44; the former corresponds to the enhanced fluctuations near the AFM−PM boundary, whereas the latter reflects the effective mass enhancement near the AFM−AFI transition (cf. Figure 1). Ultimately, however, the widening of the bands with increasing x becomes dominant, leading to a reduction in carrier mass and γ.

The theory specified in section V shows that the linear contribution to the specific heat at low temperature is given by the relation

$$\gamma/T = \gamma_0 T/2(l - I^2) \tag{4.2}$$

where

$$\gamma_0 = 2\pi^2 k_B{}^2 \rho^o(\epsilon_f)/3 \tag{4.3}$$

is the Sommerfeld expression for the heat capacity of a free electron gas, $\rho^o(\epsilon_f)$ is the density of states per site per spin at the Fermi level ϵ_f, and I ($\equiv U/U_C$) is a measure of the degree of electron correlation: As the Coulomb repulsion energy U approaches the critical value U_C, at which the electrons become localized, the specific heat contribution by the electrons becomes very large. This explains the enhanced γ values of the alloys whose composition is close to the metal−insulator boundary.

C. Magnetic Properties of the $NiS_{2-x}Se_x$ System. Magnetic ordering effects in NiS_2 have been repeatedly investigated through magnetization and neutron diffraction studies. These have been previously reviewed;[1] hence, only essential background information is provided here. By neutron diffraction it was shown that magnetic ordering occurs in two steps: a transition to the antiferromagnetic state takes place in the range 40−60 K; the Néel point apparently depends on the stoichiometry ratio r discussed in section III. This step is referred to as magnetic ordering of the first kind. At 30 K a second transition to a weak ferromagnetic (actually canted antiferromagnetic) state takes place; this is referred to as magnetic ordering of the second kind and coexists with ordering of the first kind.[54−56] The magnetic moments in the two configurations are 1.0 and $0.6\mu_B$, respectively (μ_B is the Bohr magneton, cf. Figure 13).

These findings have been analyzed in terms of a model Hamiltonian which involves not only the Heisenberg exchange interactions but also includes a perturbation expansion to fourth-order terms.[54,55,57−59] These latter interactions involve closed exchange paths or rings among four nearest neighbor or nearest and next nearest neighbor Ni sites. The resulting Hamiltonian becomes quite complicated, and the corresponding energies, when minimized, give rise to a variety of stable magnetic configurations, depending on the choice of parameters. It is difficult to single out a unique configuration from among the proposed structures, but it is important to note that the fundamental fourth-order model does rationalize the experimental observations. One proposed configuration is shown in Figure 11.

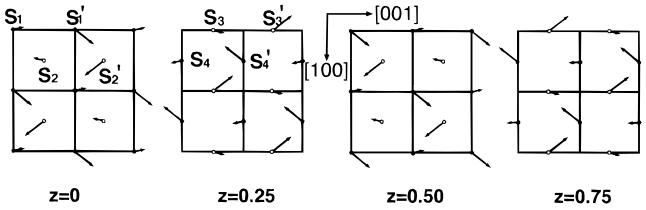

Figure 11. Projection of a possible set of spin orientations of NiS_2 onto four adjacent (001) planes. Closed or open circles denote positive or negative signs for the *z*-component. Adapted from ref 55.

The fourth order model can also be used to explain the canted spin structure at low temperatures.[54,58,60,61] Experiments with polarized neutrons[56] confirmed that the net magnetization lies along the [001] axis and has a magnitude of $0.014\mu_B$/Ni. A careful study of various possibilities identified a spin configuration identical to that depicted in Figure 11. Arguments were provided showing that the weak ferromagnetic moment is intrinsic and arises from a canting of the moments, and is not due to extrinsic phenomena, such as nonstoichiometry or to the presence of small ferromagnetic clusters. Certainly, the spin frustration effects inherent in the fcc cationic substructure will be always present and must be carefully taken into account.

Comprehensive magnetization (M) studies on NiS_2 single crystals have been carried out by Kikuchi and co-workers.[27,55] Below 30 K they report magnetization curves which conform to the relation $M = M_0 + \chi H$, where M_0 is the intrinsic magnetization, χ is the magnetic susceptibility, and $H > 10$ kG is the applied magnetic field. The field dependence of M at various temperatures and along various symmetry directions is shown in Figure 12, as is the magnetic susceptibility; the latter is essentially independent of temperature and direction. The complete magnetization curves as a function of field are of standard form and exhibit very narrow hysteresis loops of the type associated with very small net magnetic moments. An important feature of the above results is that they follow a key prediction of the theory developed by Yoshimori and Fukuda[60] that the temperature dependence of the thermally averaged spin $\langle S \rangle$ should be related to the intensity $J(hkl)$ of the diffraction peaks according to $J^{1/2}(200)$ $J(111)$. This feature confirms the applicability of Figure 11.

We now discuss the magnetic properties of the $NiS_{2-x}Se_x$ alloys. Neutron diffraction experiments on polycrystalline samples were reported by Miyadai, Sudo, and co-workers.[36,62−64] As anticipated, the substitution of Se for S weakens the magnetic ordering. This is manifested by a decline with increasing x of the calculated magnetic moments μ_{B1} and μ_{B2}, as shown in Figure 13. One also sees that the canted phase disappears around $x = 0.3$, whereas antiferromagnetic ordering persists well into the metallic region, beyond $x = 0.65$; the extrapolation of the $\mu(x)$ in the metallic phase terminates close to $x = 1$. The metal−insulator transition near $x \approx 0.45$ is reflected by an anomaly in μ_{B1}. The authors discuss the effects of Se substitution in terms of a model that involves a sphere, drawn about a central Ni atom, which encompasses 55 other Ni atoms, out to fourth nearest neighbors, and 99 associated S/Se atoms. This sphere contains all the possible exchange rings for four adjacent Ni atoms, described earlier. The

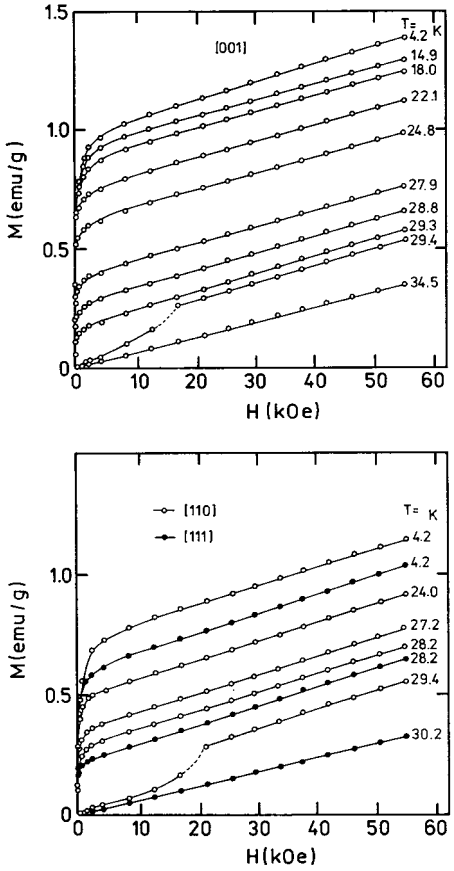

Figure 12. Magnetization curves for NiS_2 along [100] (top) and [110,111] (bottom, open circles are for the [110] direction) directions at various temperatures. Slopes of the curves represent the magnetic susceptibility. After ref 27.

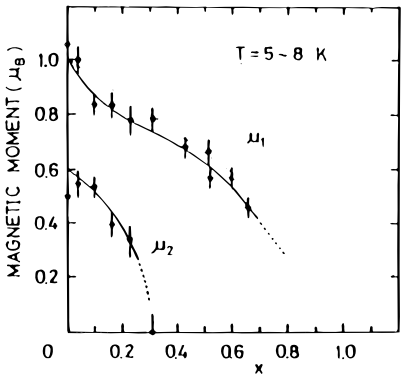

Figure 13. Composition dependence of the magnetic moments of $NiS_{2-x}Se_x$ at 5−8 K which contribute to the two types of magnetic ordering. After ref 64.

data can be interpreted as showing that when this sphere contains more than six Se atoms the exchange interactions, and hence magnetic order, are destroyed within this block of atoms, thus leading to a gradual decline of antiferromagnetism as x is increased. However, other factors, specific to the itinerant magnetism, e.g. Slater splitting, were not taken into consideration.

Magnetization studies have been carried out in several laboratories, with concordant results.[36,50,62,63] A set of complete magnetization studies was provided by Sudo and Miyadai;[64] their data for the range $0 \leq x \leq 0.55$ could again be fit to the relation $M = M_0 + \chi H$ in magnetic fields $H > 8$ kG. The χ values extracted from these data, plotted as a function of temperature, agree

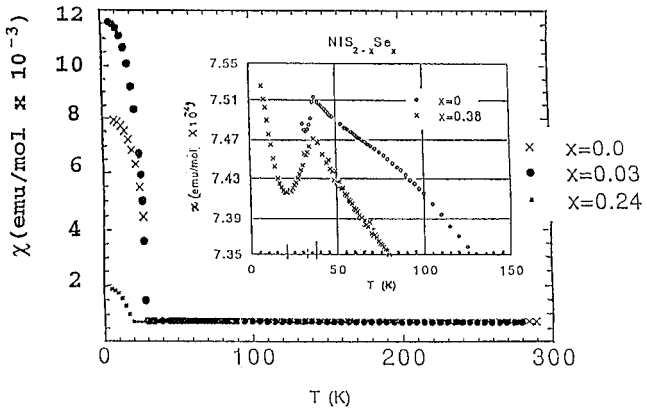

Figure 14. Magnetic susceptibility of $NiS_{2-x}Se_x$ single crystals for the low x range. Note the steeply rising curve in the ferromagnetic regime and the nearly constant value of at higher temperatures. After ref 51.

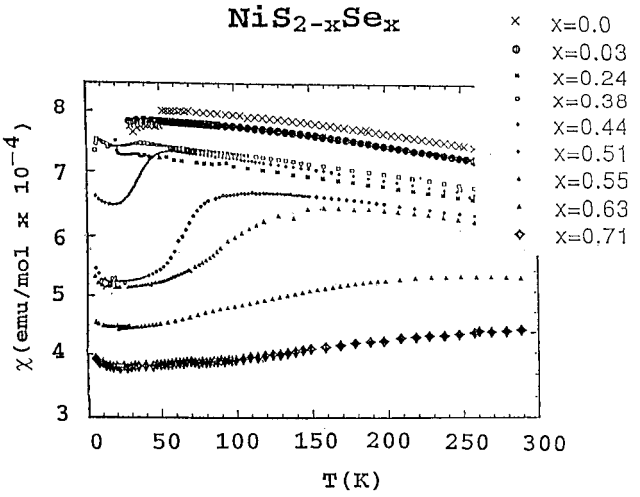

Figure 15. Magnetic susceptibility of $NiS_{2-x}Se_x$ single crystals over a wide composition range. Note the enlarged ordinate scale. After ref 51.

well with later susceptibility measurements[51] on single crystals in the range $0 \leq x \leq 0.71$, shown in Figures 14 and 15. Complementary studies[50] on polycrystalline material for $0.5 \leq x \leq 2$ are shown in Figure 16 (note that the cited composition variables must be multiplied by 2 to conform to the present notation). Examination of the data shows several features of interest: (i) the presence of weak ferromagnetism is signalled by the very steep rise of magnetic susceptibility with diminishing temperature below 30 K; the turnover at low temperature is a signature generally associated with parasitic ferromagnetism.[65] (ii) In the range above 30 K, the temperature variation is generally quite weak; a greatly magnified scale is needed to determine how χ varies with T. (iii) The nearly constant susceptibility values are quite large compared to those expected for itinerant charge carriers until compositions close to $NiSe_2$ are reached. This is characteristic of strongly correlated electron systems, as is discussed in section V. (iv) In the range $0.44 \leq x \leq 0.55$, i.e., precisely where the metal−insulator boundary is crossed, χ *rises* with temperature over a broad range between roughly 30 and 150 K, the extent of which varies with Se content of the samples. As is discussed below, we attribute this rise largely to a shrinking band width with rising T. The charge carriers then become increasingly localized,

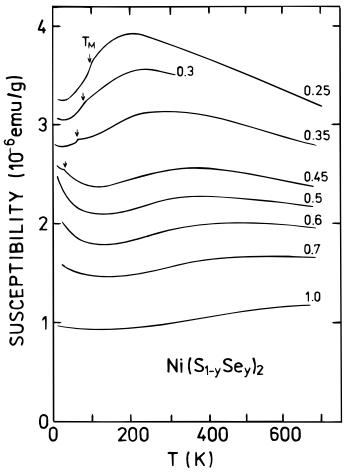

Figure 16. Magnetic susceptibility of polycrystalline $NiS_{2-x}Se_x$ for the high Se concentration range. The y values must be multiplied by 2 to convert to x values. After ref 50.

thereby displaying an increase in their magnetic moments. As mentioned earlier, Sudo[36] reported a much sharper rise of χ with T for one polycrystalline sample with $x = 0.55$ than any other investigator has been able to obtain. This clearly delineates the boundary between metal and insulator for that composition. Even in his case, however, the susceptibility is higher for the metallic (lower T) phase than on the insulating side, which directly demonstrates the effect of strong electron correlations among the itinerant carriers in the metal. (v) Ogawa[50] has deduced values of the Néel temperature from the points of inflection in his curves of Figure 16. This implies, in agreement with neutron diffraction studies, that antiferromagnetism persists well into the metallic phase, as is also evident by perusal of the phase diagram of Figure 1. (vi) As shown in Figure 17a, the Japanese group[36,63] has plotted the variation in magnetic susceptibility as a function of x at 290, 150, and 40 K; the data set of the Purdue group is also entered for comparison.[51] The discontinuity at 40 K is quite prominent. This jump was monitored by Sudo as a function of temperature, as shown in Figure 17b. One notes that the discontinuity shrinks with rising T and ends at 122 K, which Sudo takes to be the critical point of the metal−insulator boundary of the phase diagram (Figure 1). A striking overall feature of this system is the existence of a metal−insulator boundary in the antiferromagnetic phase.

D. NMR and Moessbauer Studies. There have been a number of studies involving NMR ^{77}Se measurements and Moessbauer (MB) investigations, using either ^{57}Fe or ^{61}Ni. MB studies[35,66] of ^{61}Ni in $NiS_{1.91}$−$NiS_{2.09}$ indicate small isomer shifts, with 12 lines closely bunched together. To fit the data Krill and co-workers assumed that there were two Ni sites with different hyperfine fields (HFF) and gradients, perhaps distinguished by the presence or absence of cation lattice vacancies nearby. One of the HFF and the quadrupole splitting (QS) constants change abruptly at 30 K. The Néel temperature was found to be very sensitive to the stoichiometry ratio r. MB studies have also been carried out on Fe-doped specimens. The results are to some extent unavoidably compromised by the doping process; the MB parameters depend on doping levels.[67,68] However, in one extensive study this problem was mini-

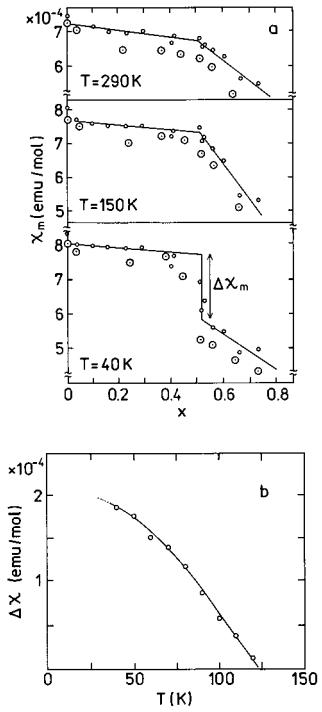

Figure 17. (a) Magnetic susceptibility of $NiS_{2-x}Se_x$ plotted as a function of composition for three temperatures. Smaller circles, ref 36; Larger circles, ref 51. (b) Plot of discontinuity of magnetic susceptibility vs temperature. Extrapolated point is interpreted as the critical point of the metal−insulator boundary. After ref 36.

mized, by working at low Fe levels, i.e., $Ni_{0.995}Fe_{0.005}S_2$.[69,70] The variation of the HFF, the angle θ between the HFF and the ⟨111⟩ direction, the QS, and the isomer shift (IS) were measured as a function of temperature. Both QS and IS varied smoothly with temperature, even across the two magnetic ordering temperatures, whereas the HFF at the ^{57}Fe nucleus dropped abruptly at 53 K; also, θ experienced a discontinuity at 30 K.

Relatively little research has been published on the alloy system. Using ^{61}Ni MB spectroscopy, Czjzek, Gautier and collaborators[71,72] detected antiferromagnetic ordering, characterized by a Néel temperature that rises up to 90 K at the metal−insulator transition (MIT) ($x = 0.55$) and then declines to zero at $x = 0.95$, consistent with the phase diagram of Figure 1. Again, at least two sets of Ni sites were needed for a good fit to the data; the presence of a nonzero QS indicated a noncollinear arrangement of the nickel moments, as in NiS_2. For the alloys $x = 0.4$, and presumably for other compositions as well, the two sets of H_{hf} and the QS coupling constant decrease linearly with rising T. This anomalous variation is explained in terms of a smooth change in the angle with temperature, quite in contrast to the abrupt discontinuity encountered in NiS_2. In the transition to the canted phase for $x = 0.2$, H_{hf} increased significantly.

Additional MB data on $Ni_{0.995}{}^{57}Fe_{0.005}S_{2-x}Se_x$[70,73] show that the two-finger pattern gradually gives way to a single broad line when x is increased from 0 to 2. The corresponding isomer shifts increase smoothly from 0.442 to 0.512 mm/s, while the QS constant of ^{57}Fe changes discontinuously at the MIT boundary. The data are fitted well by a single hyperfine field parameter which changes smoothly with x, as shown in Figure 18

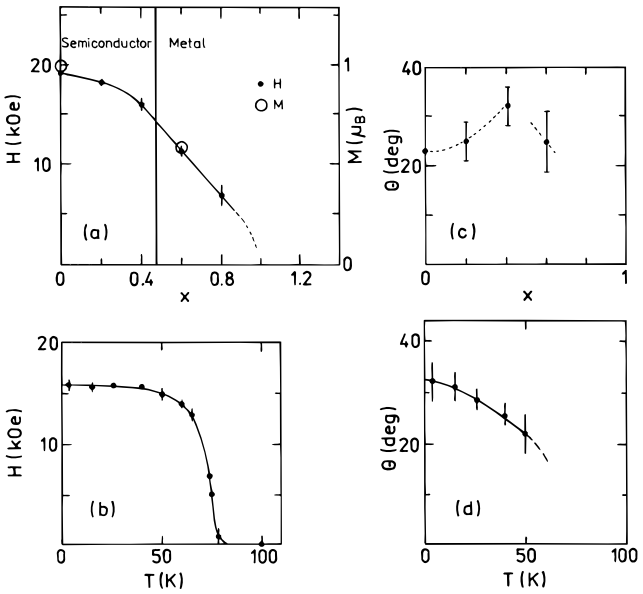

Figure 18. Hyperfine fields at the ^{57}Fe nucleus in Fe-doped $NiS_{2-x}Se_x$ as a function of x at 4.2 K (a) and as a function of temperature for $NiS_{1.6}Se_{0.4}$ (b). Also shown is the angle between the hyperfine field direction and the principal axis of the electric field gradient as a function of x (c) and as a function of temperature for $NiS_{1.6}Se_{0.4}$. After ref 70.

(4.2 K) and extrapolates to zero at $x = 1$. The change of H_{hf} and θ with x and the temperature variations of both parameters for a specimen with $x = 0.4$ are also shown. These data carry the important message that magnetic ordering does persist up to $x = 1$ and that the magnetic moments rotates toward the ⟨111⟩ direction with increasing Se content. One may speculate that the magnetic ordering may have remained undetected in neutron scattering studies because of the decreasing intensity of the magnetic reflections as x rises.

NMR measurements involving ^{77}Se[49] showed that in $NiSe_2$ the Knight shift $K = +1\%$ is independent of temperature and that the nuclear spin−lattice relaxation time, proportional to $1/T$, follows the Korringa relation, with a small exchange enhancement. This shows, consistent with the nearly T-independent value of χ, that $NiSe_2$ is a standard Pauli-paramagnetic metal with some degree of electron correlation. It would be important check whether the same type of $1/T$ dependence holds for the alloys on the magnetic side.

E. Pressure Effects. The effect of pressure (p) on various physical characteristics of the $NiS_{2-x}Se_x$ system has been repeatedly investigated. The compressibility of NiS_2, as inferred from X ray studies under moderate pressures[74] is 9.2×10^{-4}/kbar and 7.1×10^{-4}/kbar for the insulating and metallic states, respectively. From breaks in the measured neutron diffraction line intensities $J(100)$ and $J(^1/_2\ ^1/_2\ ^1/_2)$ vs T at a series of pressures Panissod et al.[75] deduce that both the Curie and the Néel temperatures of NiS_2 rise with pressure; similar conclusions were reached by Mori and Watanabe[76] on the basis of thermal expansion measurements. This reflects the increasing exchange interactions occurring when the electron energy bands are widened by increasing pressure. However, the opposite trend has been reported[77] for alloys with $x = 0.6$, based on anomalous thermal expansion measurements under pressures up to 15 kbar. This can understood by noting that in the

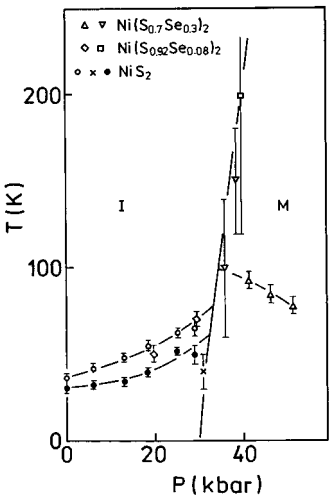

Figure 19. Phase diagram of $NiS_{2-x}Se_x$ for various x as a function of pressure. After ref 77.

insulating phase the superexchange is proportional to the hopping integral squared, whereas in the metallic phase it approaches 0 with increasing bandwidth.

A careful study of changes in structure and bond distances of NiS_2 under pressure has been published.[78] It is interesting that the S−S bond distance remains fixed as long as the system is in the insulating state, whereas it diminishes with rising $p > 46$ kbar in the metallic state; by contrast, the Ni−S distance decreases steadily.

As anticipated, raising the pressure renders NiS_2 more metallic and diminishes the activation energy for conduction.[2,35,79] One of the most striking observations is that the application of pressure on NiS_2 closely mimics the effect of increasing the Se admixture under ambient conditions. This is seen, for example, in the phase diagram of Figure 19;[77,80] there is an obvious resemblance to the phase diagram of Figure 1. This happens despite the fact that pressure diminishes lattice parameters,[74] whereas doping with Se expands the lattice. This apparent paradox can be easily resolved by noting that the principal quantity affecting the 3d is the hybridization, which rises both with Se content and pressure. These observations suggest again that the various changes in physical properties of the $NiS_{2-x}Se_x$ system reflect alterations in electronic structure rather than structural effects or rearrangements. The authors equate a 1% increase in x with a pressure increment of approximately 1.2 kbar, in reasonable concordance with estimates by Wilson.[1,2] Changes in optical properties of NiS_2 single crystals with pressure have been investigated by Takahashi,[81] who noted an increase in reflectivity with pressure due to rising electron density and effects associated with broadening of the conduction band. By contrast, the A_g Raman active frequency remains unaffected by pressure, which is taken to be due to strong electron−phonon interactions.

Quite similar conditions prevail for the $NiS_{2-x}Se_x$ system: early work by Wilson and Pitt[2] on single crystals with $x = 0$, 0.2, 0.4, 0.8 showed a sharp drop of the resistivity with rising pressure at 300 K, which ultimately effected a transition to the metallic state. For the composition range $0.7 \leq x \leq 1.2$, the application of pressure[39] reduced the resistivities somewhat but did

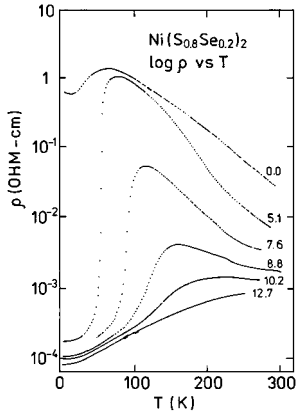

Figure 20. Electrical resistivity of $NiS_{1.6}Se_{0.4}$ as a function of temperature for various pressures listed in the figure. After ref 80.

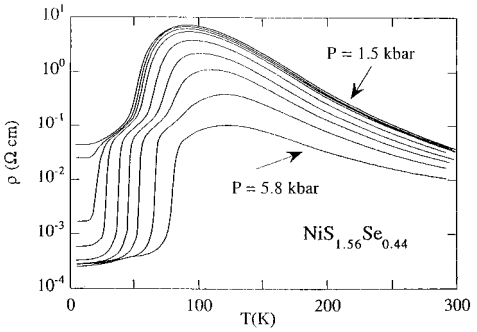

Figure 21. Electrical resistivity of $NiS_{1.56}Se_{0.44}$ as a function of temperature for various pressures 1.5 kbar $\leq p \leq$ kbar.

not greatly affect the trends in the variation of ρ with T which, at low temperatures, had the familiar $\rho = \rho_0 + AT^2$ form. The coefficient A peaked at a pressure of 9 kbar, corresponding to the value $x = 1$, in consonance with measurements cited earlier.[45] Of particular interest is Figure 20, which shows the variation in resistivity of a polycrystalline specimen with $x = 0.4$, subjected to a series of gradually increasing pressures. One should compare these findings with those of Figure 7. The evolution of both sets of data runs in parallel: with rising p the hump in the resistivity curves of Figure 20 becomes more prominent and then fades away beyond 10 kbar, while the resistivity at any given temperature drops with rising p. Precisely the same phenomenon is seen in Figure 7, when x is increased. Thus, even in the alloy system the equivalence of pressure and increased Se content is clearly manifest.

Rosenbaum and collaborators[82] have studied the electrical properties at 50 mK of single crystals with $x = 0.44$ that are insulating under ambient condition but were rendered metallic by hydrostatic pressure. The critical pressure for the transformation was 1.6 kbar, above which ρ is proportional to T^2, with $A = 0.042$ $\mu\Omega$ cm/K^2, from 5 K up to at least 16 K; however, $\rho \sim T^{1/2}$ below 1 K, which is characteristic of electronic correlations where crystalline disorder plays a dominant role. For pressures very close to the MIT the conductivity follows the unusual $T^{0.22}$ dependence, whose origin is uncertain. In Figure 21 we show preliminary measurements[82a] of the temperature variation in resistivity of one sample with $x = 0.44$. Note the two transformations engendered by rising temperature beyond 1.5 kbar: a sharp transition to an insulating state, followed by the

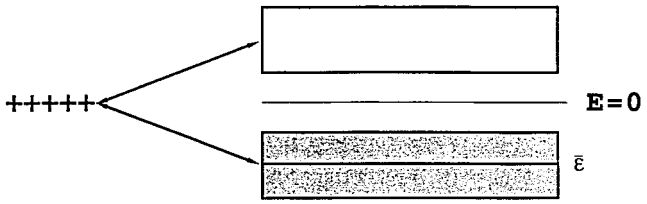

Figure 22. Energy of charge carriers (a) in the localized state, where $E = 0$ by convention, (b) in a band that is half-filled. Note that the average band energy, $\bar{\epsilon}$, is negative relative to the chosen zero of energy.

residue of the ambient peak of Figure 7b, and the subsequent dropoff in resistivity. Moreover, one should observe the very marked decline in the zero temperature resistivity ρ_0 with rising pressure, which amounts to 3 orders of magnitude. This demonstrates the unusual sensitivity of the system to small pressure effects and a relatively fast transformation to the AFM state.

V. Theoretical Overview: Effects of Electron Correlation on Physical Properties

A. Qualitative Interpretation of Experimental Findings. We rationalize the experimental observations at an elementary level by drawing on the theory of electron correlation effects. This approach is motivated by the fact that with increasing x the $NiS_{2-x}Se_x$ system evolves from a Mott−Hubbard insulator to a poor metal. In the latter regime the electrons are expected to move through the system via narrow band states with a well-defined quasimomentum $\hbar k$. The concept of quantum electron gas must then must be replaced by an interacting electron fluid. The simplest model for such a collection of carriers was developed by Brinkman and Rice[83] for zero temperature, while the basic theory for nonzero temperatures was developed by Spałek and co-workers in the period 1983−1991.[84−90] This approach is applicable to a magnetically disordered material characterized by a nondegenerate narrow band that is exactly half-filled. The procedure has recently been extended by Klejnberg and Spałek[91] to treat orbitally degenerate systems.

Intuitively, charge carriers moving in a narrow band are sluggish and thus prone to perturbations by various interactions, such that they tend to avoid each other. Nevertheless, at nonzero temperatures there is a finite probability that at any instant two electrons will temporarily reside on the same atomic site with reversed spins. At a very elementary level one assigns an interaction energy U to such an electron pair; the longer range part of the Coulomb interaction is ignored. The total Coulomb interaction energy is then given by $U\eta$, where η is the probability of double occupancy of any atomic site.

The average band (kinetic) energy of noninteracting (bare) electrons is written as $-|\bar{\epsilon}|$ taken relative to the energy of the electron localized on its parent atom with reference energy zero, as sketched in Figure 22. This average bare band energy must be modified by introducing a so-called band narrowing factor $\Phi = \Phi(\eta) < 1$, which simulates the increasing difficulty that the interacting electrons experience in moving past each other. The resultant renormalized band energy is then specified by $E_k = -\Phi|\bar{\epsilon}|$, and the total energy per electron of the interacting electron system is written as

$$E_0 = -\Phi|\bar{\epsilon}| + U\eta \tag{5.1}$$

The detailed theory that specifies $\Phi(\eta)$ and η in terms of U and the bare band width W need not concern us at the moment; what is important is that the two terms in eq 5.1 are of opposite sign. Thus, under appropriate conditions, involving strong Coulombic repulsions, the positive repulsion and negative band energies can nearly cancel out, thereby rendering E_0 small. In the limit where $\Phi(\eta) \rightarrow 0$ the electrons freeze on the atoms.

The temperature dependence of the energy can be built in by use of the standard relation $E = E_0 + \int C_v \, dT$, where C_v is the heat capacity at constant volume. For itinerant electrons one may introduce the Sommerfeld expression $C_v = \gamma T$, where γ represents the electronic contribution to the specific heat of the interacting electrons; this quantity is specified by the detailed theory.[84,85,87−90] The internal per electron then assumes the form

$$E = E_0 + (1/2)\gamma T^2 \tag{5.2}$$

The increase in energy with rising T is due to the conversion of thermal energy into electron excitations across the Fermi surface.

By similar reasoning we specify the entropy of the interacting electron system as $S = \int (C_v/T)\, dT = \gamma T$. The free energy F_i per electron of the itinerant electrons is then given as

$$F_i = E - TS = E_0 - (1/2)\gamma T^2 \tag{5.3}$$

showing that F_i diminishes parabolically with rising temperature, due to the entropic contribution.

The above situation should be contrasted with the case where one electron is localized at each atomic site. As shown in Figure 22, its energy E_l is 0 because of the adopted energy reference value; for simplicity we neglect magnetic interactions. The entropy is $S_l = k_B \ln 2$ per electron, because the electron can reside at the site in either the spin-up or the spin-down configuration (k_B is the Boltzmann constant). The free energy per electron is then given by

$$F_l = -(k_B \ln 2)T \tag{5.4}$$

which diminishes linearly with rising temperature, due to the constant entropy of the magnetic moments flipping between spin-up and spin-down states.

One can determine whether the itinerant or localized regime prevails by noting which one has the lower free energy, assuming that these two states may be regarded as distinct phases in the thermodynamic sense. The stability issue is best resolved by examining Figure 23, where we schematically depict plots of F_i (parabolas with different intercepts E_0) and F_l (straight line). As is seen, for sufficiently negative values of the intercept (curve 1) the itinerant state will always have the lower free energy and will therefore be the stable configuration over the entire temperature range. For positive E_0 (curve 2) one obtains a single intersection of the parabola with the straight line: at low T the localized state has the lower free energy. At the transition

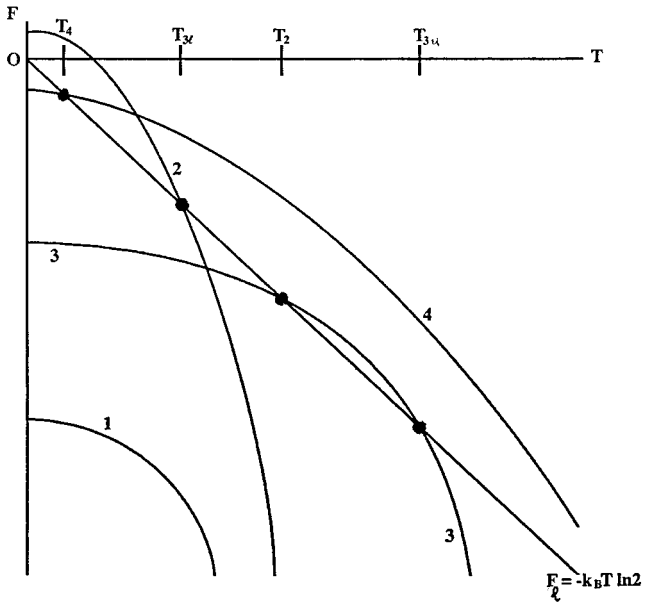

Figure 23. Schematic diagram showing the variation of the free energy F with temperature for localized electrons (straight line) and for itinerant electrons (parabolas). The various intercepts are determined by E_0.

temperature T_2 the system transforms to the itinerant regime, which has the lower free energy for all $T > T_2$. This type of transformation is very commonly encountered for many classes of materials undergoing a metal−insulator transition. Of greater interest in the present situation is curve 3, with an E_0 value that engenders a double intersection with the straight line. With rising temperature one encounters two transitions: For $T < T_{3l}$ the metallic state is stable; at T_{3l} a transition occurs to the localized regime, which is stable for $T_{3l} < T < T_{3u}$. At T_{3u} the system reenters the metallic state which then has the lower free energy for all $T > T_{3u}$. Systems with this type of reentrant metallic behavior exist: Cr-doped V_2O_3 is one such example,[92−94] Lastly, curve 4 illustrates the situation where the kinetic and potential energies are very nearly in balance, rendering E_0 slightly negative. In this case the second intersection occurs at inaccessibly high temperatures, so that effectively the system is in the metallic state at low temperatures $T < T_4$ and in the localized configuration above the transition. Clearly, this unusual situation can occur only under special conditions: because one can control the degree of electron correlation by adjustment of the Se content in the $NiS_{2-x}Se_x$ system, one is able to work in a composition range where these unusual effects become manifest. A more quantitative calculation is displayed in Figure 24, where the average value $\gamma = 24$ mJ/mol K^2 was adopted; the different parabolas correspond to different choices for E_0. By interpolation one arrives at a value of $E_0 = -259$ J/mol when a value of $T_4 = 50$ K is adopted. This compares to an energy for the solid on the order of 10^4 J/mol. This provides some insight into the balance between kinetic and potential energies which prevail for poorly conducting $NiS_{2-x}Se_x$.

One should, however, note that magnetic ordering effects and degeneracy effects are ignored. Transitions involving magnetic disordering are not covered here but are briefly dealt with below.

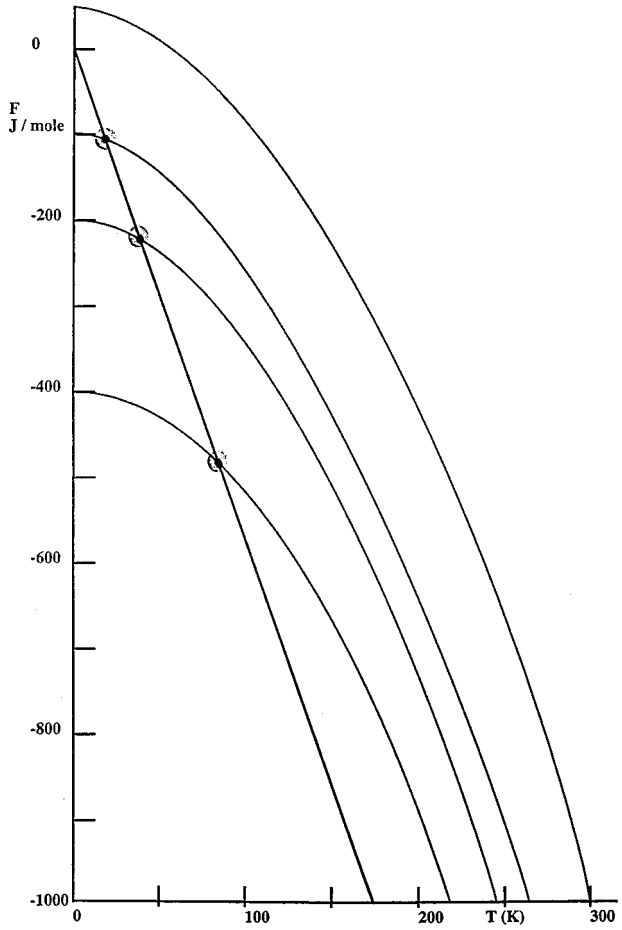

Figure 24. Calculated free energy curves as explained in the text.

Despite the very simplistic approach, the above theory does provide a rationale for the effects displayed in Figure 7b−d. In this composition range the electron correlation effects are sufficiently strong to reflect the situation of curve 4 in Figure 23. A metallic state at low temperature gives way to a crossover region in which it becomes more favorable, in terms of free energy, for the system to move toward a more localized regime. This engenders a shrinking of the bare band width W with rising temperature, to the point where a small bandgap opens up in the density of states over a small temperature interval and then locks in. This is believed to be responsible for the very steep rise of resistivity with temperature in Figure 7b−d. Ultimately, a gap of E_g is established, separating either the lower and upper Hubbard subbands, or establishing a charge transfer energy gap, Δ, depending on whether the band structure scheme of Figure 3b or 3c or 3d applies. Beyond the lock-in point the standard semiconducting regime is stabilized, which involves a fixed band gap and an exponential decline in resistivity with rising temperature.

The trend toward increased localization is also manifest in the magnetic properties. As already noted, for materials in category ii the magnetization rises with temperature in the range 50−100 K, depending on composition x. This unusual behavior may be linked to the increasing degree of localization of the electrons in that range of T, thereby increasing the magnetic moment of each ion.

The resistivity data for semiconductors in category i may be rationalized by noting Figure 7a, where in $T >$ 130 K the material acts as a semiconductor with an activation energy $E_a = 110$ meV. When magnetic ordering sets in the rise of resistivity with diminishing temperature is interrupted, but for $T < 30$ K, where the parasitic ferromagnetic regime is encountered, the materials again display semiconducting properties, characterized by a larger activation energy $E_a = 330$ meV. This is believed to arise because in the nearly antiferromagnetically ordered state a Slater gap opens up as well, as explained below, and thus adds to the correlation-induced gap already present in the magnetically disordered configuration.

Materials in categories iii and iv tend to be poor metals, as already documented in section IV.A. Correspondingly, the electronic contribution to the heat capacity is larger (ca. 25 mJ/mol K^2) than that anticipated for ordinary metals (on the order of 1−5 mJ/mol K^2), as already noted.

B. Quantitative Formulation: Hubbard and Related Models. The basic theory developed below addresses the changeover from metallic characteristics to a magnetically ordered insulating state as the temperature T is decreased. This effect is associated with the localization of the 3d electronic states of the transition metal ion (Ni^{2+} in the present case). The transition is viewed as a change from an itinerant electronic state of both $3de_g$ electrons with a definite (quasi) momentum to a localized atomic configuration in the solid. To treat this changeover one begins with the Bloch states that describe electron transfers between sites. This description is facilitated through the use of the so-called second quantization scheme: within the model described in section V.A the Hamiltonian for such a collection of electrons may be written as

$$\mathbf{H} = \sum_{ijo} t_{ij} a_{i\sigma}^{\dagger} a_{j\sigma} + U \sum_{j} n_{i\uparrow} n_{i\downarrow} - \mu N \qquad (5.5)$$

The first term represents the hopping process of an electron with spin σ from site j (where it is "annihilated" by the operator $a_{j\sigma}$) to site i (where it is "created" by the operator $a_{j\sigma}^{\dagger}$), without spin reversal; $\sigma = \pm 1 = \uparrow$ or $\downarrow$. The probability of such an event is governed by the transfer integral t_{ij}. The second term represents the Coulomb interaction energy when two electrons of opposite spins temporarily reside at the same atomic site i in the solid. Further, $n_{i\sigma} = 0,1$ is the particle number on site i with spin σ. The last term involves the chemical potential and the total, fixed number of particles, N, in the system. The site index also labels the orthogonalized atomic (Wannier) orbitals, $\Phi_i(r)$, appropriate to an electron situated on site i. In terms of this function, the transfer integral in eq 5.5 is specified by

$$t_{ij} = \int \mathrm{d}^3 r \; \Phi_i^*(r) \left[-\frac{\hbar^2}{2m} \nabla_r^2 + V(r) \right] \Phi_j(r) \qquad (5.6)$$

and the Coulomb integral is given by

$$U = \int\int \mathrm{d}^3 r \; \mathrm{d}^3 r' \; |\Phi_i(r)|^2 \left[\frac{\mathrm{e}^2}{|r - r'|} \right] |\Phi_i(r')|^2 \qquad (5.7)$$

where all undefined symbols retain their conventional significance. The transfer integral (5.6) contains a contribution from the kinetic energy, $-(\hbar^2/2m)\nabla_r^2$ of the electron, and also involves the total potential $V(r)$, which includes the parent-atom potential, $V_{at}(r - R_j)$. By contrast, U involves the electrostatic interaction between electrons of density $\rho(r) = |\Phi_i(r - R_j)|^2$, which is the same for every site i, due to the assumed translational invariance of this interaction. Usually, one sets the single particle energy $t_{ii} = 0$ in the atomic limit; then the double summation over i and j involves only terms with $i \neq j$. This implies that the ground state energy $E_0 = \langle \mathrm{H} + \mu \mathrm{N} \rangle = 0$ in the insulating (localized) state.

The chief difficulty in finding the electronic energies associated with the Hubbard Hamiltonian (5.5) is that the band-like (hopping) and Coulomb parts are of comparable magnitude. In order to localize electrons, the band states must be eliminated, i.e., rendered too costly in energy, in the sense that electrons cannot get past each other because the Coulomb repulsion energy is too high. In short, the first two terms in eq 5.5 affect each other strongly. To avoid this problem one can "renormalize" the energetics by setting up the expression

$$\mathrm{E} = \Phi \sum_{ij\sigma}{}' t_{ij} \langle a_{i\sigma}^{\dagger} a_{j\sigma} \rangle + U \sum_{i} \langle n_{i\uparrow} n_{i\downarrow} \rangle \qquad (5.8)$$

as the total energy. Here we have introduced the averages $\langle a_{i\sigma}^{\dagger} a_{j\sigma} \rangle$ and $\langle n_{i\uparrow} n_{i\downarrow} \rangle$ to simulate the effects of the corresponding terms in the Hamiltonian (5.5), and we have introduced a function Φ to modify the transfer integral t_{ij}. Next, we introduce $n \equiv \langle n_{i\uparrow} n_{i\downarrow} \rangle$ as the basic two-particle correlation function; i.e., η represents the probability of encountering a doubly occupied site; correspondingly, we expect $\Phi = \Phi(\eta)$ to be a function of η.

We ascertain the physical significance of the function Φ by carrying out a space Fourier transformation, to switch from the position to the momentum representation of the energy. Standard operations lead to the following result:

$$\langle \Phi \sum_{ij\sigma}{}' t_{ij} \langle a_{i\sigma}^{\dagger} a_{j\sigma} \rangle \rangle = \Phi \sum_{k} \epsilon_k \bar{n}_{k\sigma} \qquad (5.9)$$

where

$$\epsilon_k \equiv \frac{1}{N} \sum_{ij}{}' t_{ij} \exp[ik(R_i - R_j)] \qquad (5.10)$$

is the single particle band energy for noninteracting electrons and $\bar{n}_{k\sigma} \equiv \langle a_{k\sigma}^{\dagger} a_{k\sigma} \rangle$ is the average density of particles in the Bloch state. In the simplest case of free electrons we may set $\epsilon_k = \hbar^2 k^2/2m$, where m is the free electron mass, $\hbar \equiv h/2\pi$. The band energy for the interacting electron system may be written as $E_k = \hbar^2 k^2/2m^*$, whence $\Phi = m^*/m$. Note that for weak interactions $\Phi(\eta) \rightarrow 1$; also, $\eta \rightarrow \langle n_{i\uparrow} \rangle \langle n_{i\downarrow} \rangle = n^2/4$, where n is the average number of electrons per site. By contrast, for extremely strong electron interactions $m^* \rightarrow \infty$, $\Phi \rightarrow 0$, $E_G \rightarrow 0$, showing that the bandwidth also approaches zero and reduces to the atomic level. Φ is thus seen to

play the role of a band narrowing factor; the larger the effective mass, the smaller is Φ and the narrower is the band.

The above argument may be extended[83−87] to cover the case of a magnetically polarized material for which $\langle n_{i\uparrow}\rangle \neq \langle n_{i\downarrow}\rangle$; one then finds that ($\sigma = \uparrow, \downarrow$)

$$\Phi(\eta) = \frac{1}{n_\sigma(1-n_\sigma)}\{\sqrt{\eta}\,\sqrt{\eta_{\bar\sigma}-\eta} + \sqrt{\eta_\sigma-\eta}\,\sqrt{1-\mathrm{n}+\eta}\} \quad (5.11)$$

In the paramagnetic phase, for which $n_\uparrow = n_\downarrow$, and for the case of a half-filled band, where $n = 1$, the above reduces to

$$\Phi(\eta) = 8\eta(1-2\eta) \quad (5.11a)$$

and the band energy takes the form

$$E_G/N = \Phi(\eta)\bar\epsilon + U\eta \quad (5.12)$$

where $\bar\epsilon < 0$ is the bare electron band energy and N is the number of atomic sites. This energy must be minimized to enforce equilibrium conditions, by setting $\partial E_G/\partial\eta = 0$, $\partial^2 E_G/\partial\eta^2 > 0$, which leads to the requirements

$$\eta_0 = 1/4(1 - U/U_c) \quad (5.13a)$$

$$\Phi_0(\eta_0) = \mathrm{I} - (U/U_c)^2 \quad (5.13b)$$

$$\mathrm{E}_0 = (1 - U/U_c)^2\bar\epsilon \quad (5.13c)$$

where $\mathrm{U_c} \equiv 8|\bar\epsilon|$. For a featureless (constant) density of states the average bare electron energy is $\bar\epsilon = -W/4$ and $U_c = 2W$. One should note that U_c plays the role of a critical Coulomb interaction energy: If $U > U_c$ in eq 5.13a, η becomes negative, i.e., physically meaningless; the system then switches over to the localized configuration, because at $U = U_c$, $E = 0$, which is symptomatic of localization.

This raises the interesting question of the proper thermodynamic description of the transition. To apply to experimental data, one must now introduce the temperature T as an additional variable, since the metal−insulator transition occurs for $T > 0$. It is generally assumed that the concept of quasiparticles associated with energies E_k carries over from the $T = 0$ to the $T > 0$ domain. Thus we must adjoin to the energy function (5.8) the entropy contribution, to obtain a free energy functional of the form

$$\frac{\mathrm{F}(\eta)}{N} = \frac{1}{N}\sum_{k\sigma}\mathrm{E}_k\bar n_{k\sigma} + \mathrm{U}\eta + \frac{k_\mathrm{B}T}{N}\sum_{k\sigma}\{\bar n_{k\sigma}\ln\bar n_{k\sigma} + (1-\bar n_{k\sigma})\ln(1-\bar n_{k\sigma})\} \quad (5.14)$$

in which the $\bar n_{k\sigma}$ are specified by the Fermi−Dirac distribution function

$$\bar n_{k\sigma} = \{\exp[(E_k - \mu)/k_\mathrm{B}T] + 1\}^{-1} \quad (5.15)$$

The last term in eq 5.14 clearly represents the configurational entropy of the mobile electrons; k_B is Boltzmann's constant. The actual free energy is found through the minimization procedure

$$\partial \mathrm{F}/\partial\eta = 0 \quad \partial^2 F/\partial\eta^2 > 0 \quad (5.16)$$

The first condition leads to an equation which may be solved for $\eta = \eta(T)$; when this quantity is substituted in eq 5.14 one obtains the actual free energy. Usually it suffices to expand the result in powers of the temperature T; the first nontrivial order results were discussed in section V.A, where conditions were provided under which electron itineracy can be destabilized with rising T. Explicitly, the low-temperature expansion[88,89] leads to the result

$$\frac{F}{N} = \left(1 - \frac{U}{U_c}\right)^2 E - \frac{1}{2}\frac{\gamma_0 T^2}{1-(\mathrm{U}/U_c)^2} + \mathrm{O}(T^4) \quad (5.17)$$

where $\gamma_0 = (2/3)\pi^2 k_\mathrm{B}^2\rho(\epsilon_\mathrm{F})$ is the familiar Sommerfeld linear specific heat coefficient for bare electrons; $\rho(\epsilon_\mathrm{F})$ is the density of states per atom per spin at the Fermi energy ϵ_F. As discussed in section V.A, the free energy density of a magnetic insulator is given by $-k_\mathrm{B}T\ln 2$. At the metal−insulator phase transition this latter quantity matches eq 5.17 for the free energy density of itinerant carriers. On equating these quantities and solving for the transition temperature, one arrives at a quadratic equation which may be solved for

$$k_\mathrm{B}T_\pm = \frac{3\Phi_0}{2T^2\rho_0}\left\{\ln 2 \pm \left[(\ln 2)^2 - \frac{4\pi^2}{3}\rho_0\left|\bar\epsilon\right|\left(1-\frac{U}{U_c}\right)^2/\Phi_0\right]^{1/2}\right\} \quad (5.18)$$

As T rises, the system transforms from the itinerant to the localized state at $T = T_-$ and transforms back to the itinerant state at $T = T_+$; the theory thus predicts reentrant metallic behavior, as indicated in Figure 23, so long as T_+ is physically attainable without risking decomposition. The two transitions disappear at the critical temperature

$$k_\mathrm{B}T_\mathrm{c} = \frac{3\ln 2}{2\pi^2\rho_0}\left[1 - \left(\frac{U_\mathrm{lc}}{U_\mathrm{c}}\right)^2\right] \quad (5.19)$$

and for the lower critical U value of

$$U_\mathrm{lc} = U_\mathrm{c}\left[1 - \frac{\sqrt{3}\ln 2}{2\rho_0}\frac{1}{(\rho_0|\bar\epsilon|)^{1/2}}\right] \quad (5.20)$$

Note that for $U = U_c$, $T_c = 0$; the point ($T_c = 0$, $U_c = 0$) represents a quantum critical point at which the transition becomes continuous.

The above theory describes the transition between itineracy and localization with rising temperature in magnetically disordered systems. In reality, the $NiS_{2-x}Se_x$ phase change involves an antiferromagnetically ordered state at low temperatures. This problem is briefly dealt with in the next section.

C. Effect of Antiferromagnetic Ordering. In the simplest case (nondegenerate s-type band) of an antiferromagnetic metal which orders magnetically at the Néel point the originally half-filled band splits into two subbands, known as Slater subbands, which correspond to the reorganization of the lattice into two sublattices with reversed spins. This gives rise to a metal−

insulator transition, because at $T = 0$ the lower lying band is completely filled and the upper band is empty. When electron correlation effects are prominent, each subband is narrowed further through the Φ factor introduced in section V.B. For strong correlations, the system then undergoes a transition from the state $\Phi < 1$ to the state $\Phi = 0$; the system thereby transforms from the Slater (AFM or AFI) to the Mott (AFI) state. The itinerant-system AFI state can only prevail when the Slater gap does not depend on the quasimomentum $\hbar k$; otherwise the magnetically ordered state remains metallic along certain directions in reciprocal space or at some points on the Fermi surface. This latter scenario applies to $NiS_{2-x}Se_x$, as is clear from inspection of Figures 7. However, the physical cause for the existence of such gap zeros has not yet been identified. Two possibilities come to mind: (i) spin frustration effects; i.e., the Ni sublattice is in the fcc configuration, the resulting magnetic frustration forcing the magnetic moments into a noncollinear structure, or (ii) the gap is of nonstandard (i.e., k dependent) form.

For the antiferromagnetic configuration the total ground state energy density may be written as[95]

$$\frac{E_0^{AF}}{N} = -\frac{1}{N}\sum_k{}'[\sqrt{(\Phi\epsilon_k)^2 + \Delta_k{}^2} + U\eta + \Delta_k m] \quad (5.21)$$

where m is the sublattice magnetization, and Δ_k is the effective staggered molecular field. If $\Delta_k = 0$, the system reverts to a configuration similar to a paramagnetic state, the difference being that only a fraction of the electrons are thermally excited at temperatures well below the Néel point. The molecular field is a consequence of electron correlations, although we do not elaborate on it here. A system close to localization will transform with rising T to an antiferromagnetic insulating state, when $\Phi \rightarrow 0$; at still higher T the system then transforms into either a paramagnetic insulating or a reentrant paramagnetic metallic state, depending on whether $T_N < T_+$ or $T_N > T_+$, respectively. The T_- temperature corresponds to the AFM−AFI transition.

D. Other Characteristic Physical Effects Arising from Electron Correlations. Electron correlation effects induced by strong on-site Coulomb interactions between charge carriers give rise to several characteristic properties of the metallic state close to the Mott localization limit. Some of these are listed below under separate headings.

(1) A large T^2 term in the electrical resistivity. This is observed experimentally, as shown in Figure 25 for the alloys with $0.44 \leq x \leq 0.71$; the residual resistivity ρ_0 has been subtracted out. According to standard theory one anticipates that $\rho - \rho_0 = AT^2$. We observe two straight line regions for $T < T_N$ and $T > T_N$, respectively. The fact that the coefficient A is smaller for $T < T_N$ indicates that the Fermi surface is partially gapped in the AFM state, which results in a smaller density of excited carriers. This, in turn, means that the Slater (magnetic) gap is k-dependent and has nodes. This suggestion should be verified and studied carefully. With rising x the AT^2 term steadily diminishes as the correlation effects die down. By contrast, A is largest as the localization limit is reached.

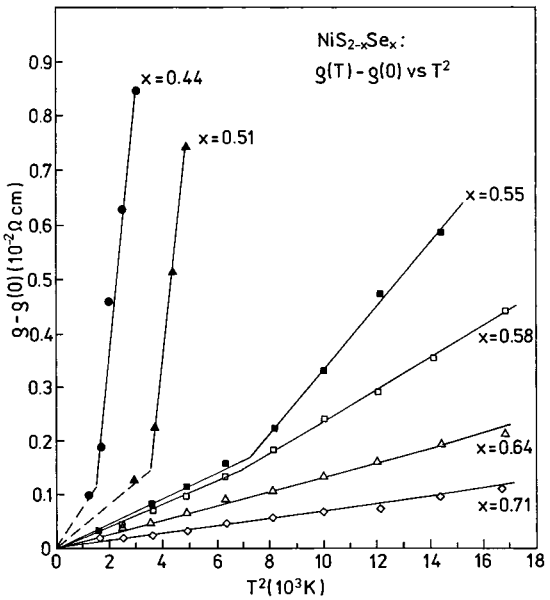

Figure 25. Temperature dependence of $(T)-(0)$ for several $NiS_{2-x}Se_x$ specimens. The coefficient A (slope of the lines) differs for the different magnetic phases.

(2) A large value of the linear term in the specific heat: This quantity is expected to increase as $(1 - (U/U_c)^2)^{-1}$ for correlated electrons (see eq 4.2); thus γ should rise indefinitely when localization is approached through reduction in x from the metallic side. The existing data confirm such a trend: typical values of γ are in the 25−35 mJ/K^2 mol range, which are decisively higher than values of 1−5 mJ/K^2 mol for ordinary metals. Very large γ values are not reached since the AFM−AFI first-order transition intervenes, making it impossible to approach the limiting value U_c. Such behavior was explicitly observed in nonstoichiometric $V_{2(1-y)}O_3$ system.[82a] Furthermore, the presence of the T ln T contribution, arising from spin fluctuations, to the specific heat in the PM phase should be tested carefully.

(3) A large value in the magnetic susceptibility χ_0: In zero-order the magnetic susceptibility does not vary dramatically with temperature except near the metal−insulator boundary. Values for materials with significant correlation effects are substantially larger than the magnetic susceptibilities of ordinary metals. Indeed, the Pauli paramagnetism of standard metals is considerably exceeded in the $NiS_{2-x}Se_x$ system, with χ_0 declining as x rises, in accord with expectations.

(4) A significant T^2 contribution to the magnetic susceptibility: According to theory[88,89] one expects that $\chi_0 = \chi_0(1 - BT^2)$ for the metallic regime. This is reflected in the data displayed in Figure 26 for the temperature dependence of **M** for the $0.44 \leq x \leq 0.51$ composition range, the susceptibility at $T = 0$ having been subtracted out. The coefficient B clearly diminishes with increasing x, signalling again the gradual evolution of the system toward the normal metallic state with increasing Se content (note the scale change for the data with $x = 0.55$).

(5) The phenomenon of metamagnetism: It has been recognized[96−98] that electron correlations lead to spectacular effects in the presence of sufficiently intense magnetic fields. Among these is the phenomenon of metamagnetism which results in a first-order transition

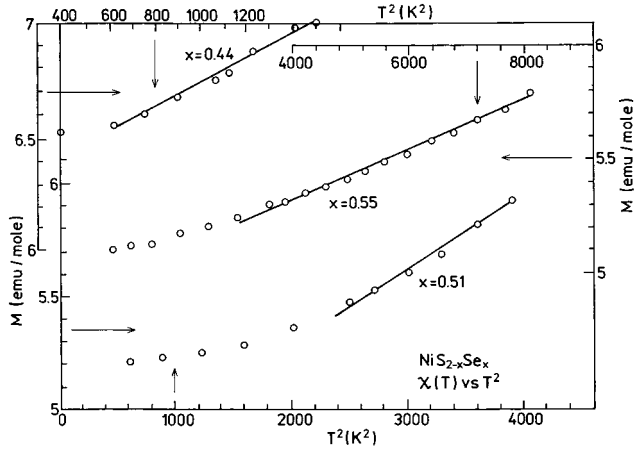

Figure 26. Magnetization of $NiS_{2-x}Se_x$ samples vs T^2. The slope of these lines yields the B value discussed in the text.

at a given field from the unsaturated to the saturated ferromagnetic state. Also, the low-field dependence of magnetization is concave, in contrast to the ordinary Brillouin law. The other is a strong magnetic field dependence of γ (The effective mass is then spin-split!). Neither of these effects has so far been observed experimentally in the $NiS_{2-x}Se_x$ system.

(6) The role of degeneracy and the Hund's rule coupling J: This problem has been studied in detail recently.[91] Hund's rule induces a first-order transition even at $T = 0$. The other features of the transition are very similar to those in the nondegenerate case (note that $J \sim 0.2U$). Obviously, Hund's rule exchange facilitates localization, thereby reducing the critical value U_c.

VI. Conclusion

The $NiS_{2-x}Se_x$ system serves as a very good testing ground for electron correlation effects which have been the subject of many recent theoretical developments. This situation arises because over a limited composition range of $0.4 \leq x \leq 0.55$ one can vary the degree of electron correlation through adjustment of the S/Se content, while leaving the cation sublattice intact. In the foregoing we have reviewed the extensive research over the last three decades involving the synthesis, single crystal growth, sample characterization, electrical, magnetic, and thermal measurements, structural studies, optical investigations, Moessbauer and NMR measurements, and other related work. We have attempted to provide a simple theoretical framework for the interpretation of these results. A key feature is the demonstration that the various theoretical predictions manifesting electron correlation effects have been verified: the enhancement of the electronic specific heat and of the Pauli paramagnetic susceptibility, a very large contribution to the electrical resistivity arising from electron-electron scattering, and the opening up of a band gap in the density of states with rising temperature. Additionally, it is stressed that the band structure of these alloys is quite complex and that several types of charge carrier participate in the electron transport process.

On the basis of the above, the long-standing problem concerning the nature of the electron states is being resolved. Because of the metal−insulator transition of the Mott−Hubbard type, as in $NiS_{2-x}Se_x$, the magnetic electrons are either localized or itinerant; no intermediate state is possible. However, the experimental verification of the actual electronic state in the metallic phase depends on the time scale of the measurement, τ_m, compared to the hopping time $\tau_B \sim \hbar/\Phi|\bar{\epsilon}| \sim 1/[1-(U/U_c)^2]$ of electrons transferring between neighboring sites. Obviously, when $\tau_m \ll \tau_B$ the electrons will appear as localized on atoms. Additionally, the band splitting into the Hubbard subbands, even in the absence of the magnetism, is of fundamental importance and explains why systems with an odd number electrons (e.g. CoO or MnO) remain insulating in the paramagnetic state. In the limit of strong correlations ($U \gg W, \Delta$) the nature of antiferromagnetic state is understood, at least qualitatively, in terms of superexchange or kinetic exchange effects (this latter topic has been not been taken up in this review).

What has not yet been resolved in the correlated electron systems is the proper role of orbital ordering in orbitally degenerate systems (viz. manganites as a prime example). This problem, as well as the properties of non-Fermi liquids in the presence of atomic disorder, are new fields of endeavor that await resolution, as is also emphasized in related reviews (refs 99 and 100). This is particularly so in low-dimensional systems such as high-temperature superconductors, where the concept of metal as a Landau Fermi liquid is now being questioned.[101]

Acknowledgment. This review was undertaken with support of the Committee for Scientific Research (KBN), Grant No. 2PO3B 129 12, and of the National Science Foundation, Grant DMR 96-12130. The authors wish to thank Dr. Robert Podsiadty for his skillful technical assistance in the preparation of the final document.

References

(1) Wilson, J. A. *The Metallic and Non-Metallic States of Matter*; Edwards, P. P. and Rao, C. N. R., Eds., Taylor and Francis, London, 1985; pp 215ff.
(2) Wilson, J. A.; Pitt, G. D. *Philos. Mag.* **1971**, *23*, 1297.
(3) Bither, T. A.; Bouchard, R. J.; Cloud, W. H.; Donohue, P. C.; Siemons, W. J. *Inorg. Chem.* **1968**, *7*, 2208.
(4) Bouchard, R. J. *J. Cryst. Growth*. **1968**, *2*, 40.
(5) Bouchard, R. J.; Gillson, J. L.; Jarrett, H. S. *Mater. Res. Bull.* **1973**, *8*, 489.
(6) Jarrett, H. S.; Bouchard, R. J.; Gillson, J. L.; Jones, G. A.; Marcus, S. M.; Weiher, J. F. *Mater. Res. Bull.* **1973**, *8*, 877.
(7) Yao, X.; Kuo, Y.-K.; Powell, D. K.; Brill, J. W.; Honig, J. M. *Phys. Rev. B* **1997**, *56*, 7129.
(8) Goodenough, J. B. *J. Solid State Chem.* **1971**, *3*, 26.
(9) Goodenough, J. B. *J. Solid State Chem.* **1972**, *5*, 144.
(10) Khan, M. A. *J. Phys. C: Solid State Phys.* **1976**, *9*, 81.
(11) Bullett, D. W. *J. Phys. C: Solid State Phys.* **1982**, *15*, 6163.
(12) Lauer, S.; Trautwein, A. X.; Harris, F. E. *Phys. Rev. B* **1984**, *29*, 6774.
(13) Bocquet, A. E.; Mizokawa, T.; Saitoh, T.; Namatame, H.; Fujimori, A. *Phys. Rev. B* **1992**, 3771.
(14) Bocquet, A. E.; Mayima, K.; Mizokawa, T.; Fujimori, A.; Miyadai, T.; Takahashi, H.; Môri, M.; Suga, S. *J. Phys. Condens. Matter* **1996**, *8*, 2389.
(15) Zaanen, J.; Sawatzky, G. A.; Allen, J. W. *Phys. Rev. Lett.* **1985**, *55*, 418.
(16) Ohsawa, A.; Yamamoto, H.; Watanabe, H. *J. Phys. Soc. Jpn.* **1974**, *37*, 568.
(17) Li, E. K.; Johnson, K. H.; Eastman, D. E.; Freeouf, J. L. *Phys. Rev. Lett.* **1974**, *32*, 470.
(18) Krill, G.; Amamou, A. *J. Phys. Chem. Solids* **1980**, *41*, 531.
(19) Folkerts, W.; Sawatzky, G. A.; Haas, C.; DeGroot, R. A.; Hillebrecht, F. U. *J. Phys: Solid State Phys.* **1987**, *20*, 4135.
(20) Folmer, J. C. W.; Jellinek, F.; Calis, G. H. M. *J. Solid State Chem.* **1988**, *72*, 137.

(21) Matsuura, A. Y.; Shen, Z.-X.; Dessau, D. S.; Park, C.-H.; Thio, T.; Bennett, J. W.; Jepsen, O. *Phys. Rev. B* **1996**, *53*, R7584.
(22) Fujimori, A.; Mamiya, K.; Mizokawa, T.; Miyadai, T.; Sekiguchi, T.; Takahashi, H.; Môri, N.; Suga, S. *Phys. Rev. B* **1996**, *54*, 16329.
(23) Delafosse, D.; Barret, P. C. R. *Compt. Rend. Acad. Sci.* (*Paris*) **1960**, *251*, 2964.
(24) Bonneau, P. R.; Shibao, R. K.; Kaner, R. B. *Inorg. Chem.* **1990**, *29*, 2511.
(25) Panigrahi, J. C.; Krushna Panda, R. *Mater. Lett.* **1991**, *12*, 112.
(26) Henshaw, G.; Parkin, I. P.; Shaw, G. A. *J. Chem. Soc. Dalton Trans.* **1997**, 231.
(27) (a) Kikuchi, K. *J. Phys. Soc. Jpn.* **1979**, *47*, 484. (b) Krabbes, G.; Oppermann, H. *Z. Anorg. Allg. Chem.* **1984**, *511*, 19.
(28) Scheel, H. J. *J. Cryst. Growth* **1974**, *24/25*, 669.
(29) Tanaka, U.; Komori, T.; Ishizawa, N.; Marumo, F.; Noda, Y. *J. Cryst. Growth* **1993**, *129*, 683.
(30) Yao, X.; Honig, J. M. *Mater. Res. Bull.* **1994**, *29*, 709.
(31) Yao, X.; Ehrlich, S. N.; Liedl, G.; Honig, J. M. *The Metal Nonmetal Transition Revisited*; Edwards, P. P., Rao, C. N. R., Eds.; Taylor & Francis, London, 1995; pp 127ff.
(32) Yao, X.; Honig, J. M.; Hogan, T.; Kannewurf, C.; Spałek, J. *Phys. Rev. B* **1996**, *54*, 17469.
(33) Gautier, F.; Krill, G.; Lapierre, M. F.; Robert, C. *Solid State Commun.* **1972**, *11*, 1201.
(34) Gautier, F.; Krill, G.; Lapierre, M. F.; Robert, C. *J. Phys. C Solid State Phys.* **1973**, *6*, L320.
(35) Krill, G.; Lapierre, M. F.; Gautier, F.; Robert, C.; Czjzek, G.; Fink, J.; Schmidt, H. S. *J. Phys. C. Solid State Phys.* **1976**, *9*, 761.
(36) Sudo, S. *J. Magn. Magn. Mater.* **1992**, *114*, 57.
(37) Lemos, V.; Gualberto, G. M.; Salzberg, J. B.; Cerderia, F. *Phys. Stat. Sol.* **1980**, *(b) 100*, 755.
(38) Stingl, Th.; Müller, B.; Lutz, H. D. *J. Alloys Compd.* 1992, *184*, 275.
(39) Kamada, M.; Mōri, N.; Mitsui, T. *J. Phys. Soc. C: Solid State Phys.* **1977**, *10*, L643.
(40) Ogawa, S. *Physica* **1977**, *86−88B*, 997.
(41) Kwizera, P.; Dresselhaus, M. S.; Adler, D. *Phys. Rev. B* **1980**, *21*, 2328.
(42) Miyadai, T.; Saitoh, M.; Tazuke, Y. *J. Magn. Magn. Mater.* **1992**, *104−107*, 1953.
(43) Takagi, H.; Eisaki, H.; Uchida, S.; Cava, R. J. *Spectroscopy of Mott Insulators and Correlated Metals*; Fujimori, A., Tokura, Y., Eds.; Springer Ser. Solid-State Sci., 1995; *Vol.* 119, pp 185.
(44) Yao, X.; Ehrlich, S.; Liedl, G.; Hogan, T.; Kannewurf, C.; Honig, J. M. *Mater. Res. Soc. Proc.* **1997**, *453*, 291.
(45) Miyasaka, S.; Takagi, H.; Sekine, Y.; Takahashi, H.; Mōri, N.; Cava, R. J. Submitted for publication.
(46) Thio, T.; Bennett, J. W. *Phys. Rev. B* **1994**, *50*, 10574.
(47) Harman, T. C.; Honig, J. M. Thermoelectric and Thermomagnetic Effects and Applications; McGraw-Hill: New York, 1967; Chapters 3, 4.
(48) Ogawa, S. *J. Phys. Soc. Jpn.* **1976**, *41*, 462.
(49) Inoue, N.; Yasuoka, H.; Ogawa, S. *J. Phys. Soc. Jpn.* **1980**, *48*, 850.
(50) Ogawa, S. *J. Appl. Phys.* **1979**, *50*, 2308.
(51) Yao, X.; Kuo, Y.-K.; Powell, D. K.; Brill, J. W.; Honig, J. M. *Phys. Rev. B* **1997**, *56*, 7129.
(52) Sudo, S.; Nishioka, T.; Miyako, Y.; Miyadai, T. *J. Phys. Soc. Jpn.* **1986**, *55*, 1806.
(53) Miyadai, T.; Tazuke, Y.; Kinouchi, S.; Nishioka, T.; Sudo, S.; Miyako, Y.; Watanabe, K.; Inoue, K. *J. Phys. Coll.* **1988**, *49*, C8−187.
(54) Miyadai, T.; Takizawa, K.; Nagata, H.; Ito, H.; Miyahara, S.; Hirakawa, K. *J. Phys. Soc. Jpn.* **1975**, *38*, 115.
(55) Kikuchi, K.; Miyadai, T.; Fukui, T.; Ito, H.; Takizawa, K. *J. Phys. Soc. Jpn.* **1978**, *44*, 410.
(56) Kikuchi, K.; Miyadai, T.; Ito, H.; Fukui, T. *J. Phys. Soc. Jpn.* **1978**, *45*, 444.
(57) Yoshimori, A.; Inagaki, S. *J. Phys. Soc. Jpn.* **1978**, *44*, 101.
(58) Yosida, K.; Inagaki, S. *J. Phys. Soc. Jpn.* **1981**, *50*, 3268.
(59) Yoshimori, A.; Inagaki, S. *J. Phys. Soc. Jpn.* **1981**, *50*, 769.
(60) Yoshimori, A.; Fukuda, H. *J. Phys. Soc. Jpn.* **1979**, *46*, 1663.
(61) Kikuchi, K.; Miyadai, T.; Ito, Y. *J. Magn. Magn. Mater.* **1980**, *15−18*, 485.
(62) Miyadai, T.; Sudo, S.; Takisawa, K. *J. Phys. Soc. Jpn.* **1983**, *52*, 3308.
(63) Miyadai, T.; Sudo, S.; Tazuke, Y.; Mori, N.; Miyako, Y. *J. Magn. Magn. Mater.* **1983**, *31−34*, 337.
(64) Sudo, S.; Miyadai, T. *J. Phys. Soc. Jpn.* **1985**, *54*, 3934.
(65) Carlin, R. L. *Magnetochemistry*; Springer Verlag: Berlin, 1986; pp 142ff.
(66) Czjzek, G.; Fink, J.; Schmidt, H.; Krill, G.; Gautier, F.; Lapierre, M. F.; Robert, C. *J. Phys. Coll.* **1974**, *35*, C6−621.
(67) Ward, J. B.; Howard, D. G. *J. Appl. Phys.* **1976**, *47*, 388.
(68) McCann, V. H.; Ward, J. B. *J. Phys. Chem. Solids* **1977**, *38*, 991.
(69) Nishihara, Y.; Ogawa, S.; Waki, S. *J. Phys. Soc. Jpn.* **1975**, *39*, 63.
(70) Nishihara, Y.; Ogawa, S.; Waki, S. *J. Phys. C: Solid State Phys.* **1978**, *11*, 1935.
(71) Gautier, F.; Krill, G.; Lapierre, M. F.; Panissod, P.; Robert, C.; Czjzek, G.; Fink, J.; Schmidt, H. *Phys. Lett.* **1975**, *53A*, 31.
(72) Czjzek, G.; Fink, J.; Schmidt, H.; Krill, G.; Lapierre, M. F.; Pannisod, P.; Gautier, F.; Robert, C. *J. Magn. Magn. Mater.* **1976**, *3*, 58.
(73) Nishihara, Y.; Ogawa, S. *J. Chem. Phys.* **1979**, *71*, 3796.
(74) Endo, S.; Mitsui, T.; Miyadai, T. *Phys. Lett.* **1973**, *46A*, 29.
(75) Panissod, P.; Krill, G.; Vettier, C.; Madar, R. *Solid State Commun.* **1979**, *29*, 67.
(76) Mori, N.; Watanabe, T. *Solid State Commun.* **1978**, *27*, 567.
(77) Mori, N.; Takahashi, H. *J. Magn. Magn. Mater.* **1983**, *31−34*, 335.
(78) Fujii, T.; Tanaka, K.; Marumo, F.; Noda, Y. *Miner. J.* **1987**, *13*, 448.
(79) Mori, N.; Mitsui, T.; Yomo, S. (Proc. 4th Int. Conf. High Pressure Kyoto, 1974 pp 295ff) *Solid State Commun.* **1973**, *13*, 1083.
(80) Mori, N.; Kamada, M.; Takahashi, H.; Comi, G.; Susaki, S. *Solid State Physics Pressure: Recent Adv. Anvil Devices* **1984**, 247.
(81) Takahashi, H. *J. Magn. Magn. Mater.* **1986**, *54−57*, 1019.
(82) Husmann, A.; Jin, D. S.; Zastavker, Y. V.; Rosenbaum, T. F.; Yao, X.; Honig, J. M. *Science* **1996**, *274*, 1874. (a) Rosenbaum, T. F. In *Metal Insulator Transitions Revisited*, Edwards, P. P., Rao, C. N. R., Eds.; Taylor Francis: London, 1995, p 123.
(83) Brinkman, W. F.; Rice, T. M. *Phys. Rev. B* **1970**, *2*, 1324.
(84) Spałek, J.; Oleś, A. M.; Honig, J. M. *Phys. Rev. B* **1983**, *28*, 6802.
(85) Spałek, J.; Honig, J. M.; Datta, A. *Phys. Rev. B* **1986**, *33*, 4819.
(86) Spałek, J.; Honig, J. M.; Acquarone, M.; Datta, A. *J. Magn. Magn. Mater.* **1986**, *54−57*, 1335.
(87) Spałek, J.; Datta, A.; Honig, J. M. *Phys. Rev. Lett.* **1987**, *59*, 728.
(88) Spałek, J.; Kokowski, M.; Honig, J. M. *Phys. Rev. B* **1989**, *39*, 4175.
(89) Spałek, J.; Kokowski, M.; Datta, A.; Honig, J. M. *Solid State Commun.* **1989**, *70*, 911.
(90) Datta, A.; Honig, J. M.; Spałek, J. *Phys. Rev. B* **1991**, *44*, 8459.
(91) Klejnberg, A.; Spałek, J. *Phys. Rev B* **1998**, *57*, 12041.
(92) McWhan, D. B.; Rice, T. M.; Remeika, J. P. *Phys. Rev. Lett.* **1969**, *23*, 1384.
(93) McWhan, D. B.; Menth, A.; Remeika, J. P.; Brinkman, W. F.; Rice, T. M. *Phys. Rev. B* **1973**, *7*, 1920.
(94) Kuwamoto, H.; Honig, J. M.; Appel, J. *Phys. Rev. B* **1980**, *26*, 2626.
(95) Spałek, J. *J. Solid State Chem.* **1990**, *88*, 70.
(96) Spałek, J.; Gopalan, P. *Phys. Rev. Lett.* **1990**, *64*, 2823.
(97) Korbel, P.; Spałek, J.; Wójcik, W.; Acquarone, M. *Phys. Rev. B* **1995**, *52*, R2213.
(98) Spałek, J.; Korbel, P.; Wójcik, W. *Phys. Rev. B* **1997**, *56*, 971.
(99) Georges, A.; Kotliar, G.; Krauth, W.; Rozenberg, M. *Rev. Mod. Phys.* **1996**, *68*, 13.
(100) Imada, M.; Tokura, Y.; Yoshimori, A. To be published.
(101) Anderson, P. W. *The Theory of Superconductivity in the High-T_c Cuprates*; Princeton, Princeton University Press: 1997.

CM9803509